5-1-2012

Synthesis, Structure, and Characterization of Hybrid Solids Containing Polyoxometalates and Ruthenium Polypyridyl Complexes

Yanfen Ll
Western Kentucky University, yan-fen.li@topper.wku.edu

SYNTHESIS, STRUCTURE, AND CHARACTERIZATION OF HYBRID SOLIDS CONTAINING POLYOXOMETALATES AND RUTHENIUM POLYPYRIDYL COMPLEXES

A Thesis
Presented to
The Faculty of the Department of Chemistry
Western Kentucky University
Bowling Green, Kentucky

In Partial Fulfillment
Of the Requirements for the Degree
Master of Science

By
Yanfen Li

May 2012

SYNTHESIS, STRUCTURE, AND CHARACTERIZATION OF HYBRID SOLIDS CONTAINING POLYOXOMETALATES AND RUTHENIUM POLYPYRIDYL COMPLEXES

Date Recommended 4.18.2012

Dr. Bangbo Yan, Director of Thesis

Dr. Kevin Williams

Dr. Matthew Nee

Dean, Graduate Studies and Research Date 12-May-2012

ACKNOWLEDGEMENTS

I very much appreciate everyone who has supported my research and made this thesis possible. First and foremost, I would like to thank God who has guided me through this whole journey. I would like to express my sincerest gratitude to my research advisor Dr. Bangbo Yan for his guidance, advice, knowledge, encouragement, motivation and moral support throughout my Master's study at Western Kentucky University. In particular, his devoted attitude in research and insight idea impressed me deeply. He has always been very supporting and encouraging to new ideas. He has taught me that everything was possible, so I have to open my mind and think widely. He spent a lot of time teaching me about Uv-Vis spectroscopy, Fluorescence spectroscopy, and several crystal structure softwares. He was always willing to help and patiently answer all of my questions. My thesis and my Master's degree would not have been written or completed without his selfless support and ingenuity.

I would like to thank Dr. Sean Parkin at the University of Kentucky and Dr. Aaron Celestian at Western Kentucky University. They helped me analyze the crystal structures of new phases by using Single crystal X-ray diffraction. In particular, Dr. Celestian, Aaron was always being so encouraging and nice to me. He also taught me Roman Spectroscopy, Powder X-ray diffraction, Single crystal X-ray diffraction and Simultaneous Thermogravimetric and Differential Thermal Analysis.

I am grateful for Pauline Norris' help with Elemental Analysis in this project. I would like to thank Dr. Quentin Lineberry for his help with Simultaneous Thermogravimetric and Differential Thermal Analysis.

I would like to thank all my colleagues/friends Raj Vakiti, Eric Vanover, Lin Zhu, Yaowen Cui and Kelin Wang, for their constant support and encouragement.

I appreciate the financial support provided to me by the Chemistry Department at Western Kentucky University. I would like to thank all the faculty and staff of the Department of Chemistry for their support in my graduate career at Western Kentucky University.

Last but not least, I am fully indebted to my parents, my husband and my American grandparents, who were always there whenever I needed their support and encouragement to achieve my goal. I am so proud of you.

TABLE OF CONTENTS

LIST OF FIGURES

LIST OF TABLES

SYNTHESIS, STRUCTURE, AND CHARACTERIZATION OF HYBRID SOLIDS CONTAINING POLYOXOMETALATES AND RUTHENIUM POLYPYRIDYL COMPLEXES

Yanfen Li May 2012 73 Pages

Directed by: Dr. Bangbo Yan, Dr. Kevin Williams, and Dr. Matthew Nee

Department of Chemistry Western Kentucky University

Polyoxometalates (POMs), which are inorganic metal oxide cluster anions with discrete structures, have been extensively studied in recent years due to their large variety of applications such as medicine, biology, catalysis, material sciences and chemical analysis. Ruthenium polypyridyl complexes have been extensively studied for their applications as photosensitizers in solar energy conversion and photoelectronic materials. Recently, ruthenium heterocyclic ligand complex-based building blocks have been used for the synthesis of hybrid organic-inorganic solids through the self-assembly. We are interested in the synthesis of ruthenium polypyridyl complexes and polyoxometalate anions through different ways such as coordination bonds, hydrogen bonds and ionic bonds to form hybrid organic-inorganic solids. Here, we report four novel hybrid organic-inorganic compounds, $[Ru(2,2'\text{-}bpy)_3]_2[SiW_{12}O_{40}]$ (**1**), $[Ru(2,2'\text{-}bpy)_2(CH_3CN)_2]_2[SiW_{12}O_{40}]$ (**2**), $[Ru(2,2'\text{-}bpy)_3][W_6O_{19}]$ (**3**), and $[Ru(2,2'\text{-}bpy)_3]_2[Mo_8O_{26}]\cdot 5H_2O$ (**4**)), (2,2'-bpy = 2,2'-bipyridine). Compounds **1**, **3**, and **4** were synthesized under hydrothermal reaction methods and compound **2** was synthesized by room temperature solution method. These solids were characterized by elemental analysis, UV-vis spectroscopy, fluorescence spectroscopy, thermogravimetric analysis, IR spectroscopy, powder X-ray diffraction, and Single crystal X-ray diffraction. X-ray

crystallographic study showed that the crystal structures of compounds **1**, **2**, **3** and **4** were constructed by Coulombic forces and supramolecular interactions. These molecular compounds were further connected and formed 3D structure through C–H···O_{POM} and other weak interactions. Spectroscopic studies demonstrated that electronic communication occurred between POMs and the sensitizers.

CHAPTER 1

Introduction

1.1 Objective

Hybrid organic-inorganic materials are attracting increasing attention due to their potential to generate unusual structures and properties by combining the features of the organic and inorganic components.[1,2] Among them, hybrid materials containing polyoxometalates (POMs) have shown fascinating electronic, optical, magnetic and catalytic properties.[3] However, little work has been done on the synthesis of hybrid organic-inorganic materials containing POMs and ruthenium complexes. Transition metal complexes such as ruthenium(II) polypyridyl complexes have been extensively studied for their applications as photoluminescent compounds and sensitizers in the interconversion of light and chemical energy.[4] Particularly, the tris-(2,2'-bipyridine)ruthenium(II) complex ($[Ru(2,2'\text{-}bpy)_3]^{2+}$) is the most widely studied transition metal complex which is capable of splitting water under visible light.[5]

In this research, the objective is to study the combination of ruthenium polypyridyl complexes and polyoxometalate anions through different ways such as coordination bonds, hydrogen bonds and ionic bonds to form hybrid organic-inorganic solids.

1.2 Hybrid Organic-Inorganic Materials

Hybrid organic-inorganic materials are materials prepared by combining organic and inorganic building blocks.[1] They are attracting increasing interest as a creative alternative for obtaining new materials with tailored structures and properties.[2] These new hybrid materials have a large variety of applications such as sensors, selective

membranes, all sorts of electrochemical devices, from actuators to batteries or super capacitors, supported catalysts or photo electrochemical energy conversion cells.[6] The most noticeable advantage of inorganic-organic hybrids is that they can favorably combine the often dissimilar properties of organic and inorganic components in one material. In addition, their diphasic structures lead to create multifunctional materials. For example, inorganic clusters or nanoparticles with specific optical, electronic or magnetic properties can be incorporated in organic polymer matrices.[7] The properties of hybrid materials are not only the sum of the individual contributions of both phases, but the role of their inner interfaces could be predominant.[8]

The nature of the bonds between organic and inorganic phases has been used to divide into two distinct classes. In Class I, organic and inorganic components are embedded by weak interphase bonding. Only electrostatic interactions, hydrogen bonds, or van der Waals interactions are involved. In Class II materials, the organic and inorganic moieties are linked together through strong chemical covalent or iono-covalent bonds.[7,9] The major challenge to synthesize organic-inorganic hybrid materials are to keep or enhance the best properties of each of the components while eliminating or reducing their particular limitations.[6]

1.3 Ruthenium Polypyridine Complexes

Ruthenium(II) polypyridyl complexes are the class of transition metal complexes which have been studied extensively due to their unique properties such as chemical stability, redox properties, excited-state reactivity, luminescence emission, and excited-state lifetime.[10] Ruthenium(II) complexes containing three 2,2'-bipyridyl ligands ($[Ru(2,2'\text{-}bpy)_3]^{2+}$) have been used extensively as a sensitizer of photochemical and

photophysical processes. They are selected for such an application based upon their strong absorption in the visible region, well-characterized photophysical properties, easily detected emission which facilitates quenching studies, solubility in aqueous media, thermal and photochemical stability, and ability to store sufficient energy for catalytic water splitting.[11]

The strong visible absorption characteristic of $[Ru(2,2'\text{-bpy})_3]^{2+}$ can be described as a metal−to−ligand charge transfer. The ruthenium (II) ion has a d^6 electron configuration and the geometry is approximately octahedral. In the ground state, all the electrons are spin paired. This is called a singlet state. $[Ru(2,2'\text{-bpy})_3]^{2+}$ has a strong ligand field. This means there is greater separation between the electronic states associated with the d-orbitals. This is important because the unoccupied π*−orbitals of the bipyridine ligands on $[Ru(2,2'\text{-bpy})_3]^{2+}$ lie between the *d*−orbital states. Electrons in the ground state can absorb photons and move to this ligand orbital. Since the electron moves from an orbital associated with the metal center to an orbital associated with the ligand, this is called a metal−to−ligand charge transfer (MLCT) transition. This particular transition is associated with a very strong absorption band at 450−460 nm that dominates the UV−vis spectrum of $[Ru(2,2'\text{-bpy})_3]^{2+}$. The MLCT transition can be written $[Ru(II)(2,2'\text{-bpy})_3]^{2+}$ + photon → $[[Ru(III)(2,2'\text{-bpy})_2]^{3+}(2,2'\text{-bpy}^{-})]^{2+*}$ where the ruthenium center is oxidized to Ru(III), and one bipyridine ligand gains a negative charge. The asterisk on the product designates this molecule as being in an excited state. These excited-state species that are eventually formed are well known to engage in both oxidative and reductive chemistry.[12]

Other ruthenium(II) polypyridyl complexes also have made an important contribution to the growth of photochemistry, photophysics, photocatalysts, electrochemistry and chemiluminescence, and to a better understanding of fundamental chemical processes (energy transfer, electron transfer).[13] For example, in the dye sensitization, ruthenium(II) complexes containing three 2,2'-bipyridyl-4,4'-dicaroxlylic acid ligands, ($Ru(bpy(COO)_2)_3^{4-}$) are used as sensitizers on nanocrystalline titania. When ruthenium complexes are employed, these cells show excellent stability, making practical applications feasible.[14] A series of acidosis (2,2'-bipyridine) complexes of ruthenium(II), for example, $Ru(2,2'\text{-}bpy)_2(N_3)_2$ and $Ru(2,2'\text{-}bpy)_2(L)(N_3)^+$ (L is acetonitrile or pyridine), have found that they can be rapidly oxidized to the corresponding ruthenium(III) either electrochemically or chemically, using Br_2 or Ce(IV). The ruthenium(III) complexes once formed undergo both thermal and light-induced decomposition reactions in acetonitrile in which net azide → to metal electron transfer occurs.[15] In the ligand-loss photochemistry, when *cis*-$[Ru(2,2'\text{-}bpy)_2(NH_3)_2]^{2+}$ is irradiated by near-UV light, it is able to covalently bind to 9-methyl- and 9-ethyl-guanine, as well as to single-stranded and double-stranded DNA following photoinduced ligand loss.[16]

The main drawbacks of the ruthenium polypyridyl complexes are the photolability in nonaqueous solvents, the occurrence of a ligand photo substitution reaction and toxic effects.[4,17] If the ruthenium polypyridyl complexes are immobilized onto solids to create new functional hybrid materials, they will facilitate both the isolation and recycling of the catalyst by filtration, thus providing environmentally cleaner processes.[18] The immobilization of ruthenium polypyridyl complexes onto solids also allows for entire samples to be addressed at sufficiently high rates to allow for transient excited state

populations to be examined.[19] These hybrid solids can be synthesized and processed by using soft chemistry routes based on: (i) the polymerization of functional organosilanes, macromonomers and metallic alkoxides; (ii) the encapsulation of organic components within sol-gel derived organosilicas or hybrid metallic oxides; (iii) self-assembly or template growth, nano-building block approaches, hydrothermally processed hybrid zeolites or microporous metal organic frameworks.[7] In our research, we are interested in self-assembly of the ruthenium polypyridyl complexes and polyoxometalates under hydrothermal conditions or routine synthetic conditions to form new hybrid organic-inorganic solid compounds.

1.4 Polyoxometalates

The remarkable chemical and physical properties of polyoxometalate anions have been of interest for many years due to their large variety of applications such as medicine, biology, catalysis, material sciences and chemical analysis.[20] Polyoxometalates belong to a large class of nano-sized early-transition-metal-oxygen-anion-clusters formed primarily by Mo, W and the Group V transition metals.[21,22] Each nano-sized assembly is accompanied by counter ions such as alkali metal cations, ammonium cation (NH_4^+), or polyalkylammonium cations.[23] Assembly of these metal-oxide structures can be achieved via stoichiometric control or pH control.[24]

$18Na_2WO_4 + 32H_3PO_4 \rightarrow Na_6[P_2W_{18}O_{62}] + 30Na[H_2PO_4] + 18H_2O$

$6Na_2WO_4 + 10HCl + 2(n\text{-}C_4H_9)_4NBr \rightarrow [(n\text{-}C_4H_9)_4N]_2[W_6O_{19}] + 10NaCl + 2NaBr + 5H_2O$

Generally, POMs can be classified into two broad groups as based on their chemical composition—isopoly anions $[M_mO_y]^{p-}$ and heteropoly anions $[X_xM_mO_y]^{q-}$ (Where M is

the addenda atom, O is the oxygen atom and X is the heteroatom, $x \leq m$).[21,22,25] Typically the isopolyanionic framework is composed of one type of metal atoms (termed 'addenda' atoms), which are produced by acid condensation of pure MoO_4^{2-} or WO_4^{2-}. A typical example is $W_{10}O_{32}^{4-}$. Heteropolyanions or 'mixed addenda' clusters, typically possess one or two hetero atoms, such as phosphorus, silicon, arsenic, iron or cobalt, which are located in the center of the framework. Typical examples are $PW_{12}O_{40}^{3-}$ and $P_2W_{18}O_{62}^{6-}$. Isopoly compounds are often much more unstable than their heteropoly compounds. However, they have high charges and basic oxygen surfaces, which mean they are attractive units for use as building blocks.[25] Heteropoly compounds are by far more important for catalysis as well as for other applications. Heteropoly acids – strong acids composed of heteropoly anions and protons as the countercations – constitute a special case of heteropoly compounds that is particularly important for catalytic applications.[23]

Historically, Berzelius is credited for reporting the first heteropoly salt, ammonium 12-molybdophosphate in 1826.[26] This heteropoly salt was later utilized by Svanberg and Struve for the gravimetric and volumetric determination of phosphorus in analytical chemistry in 1848.[27] By 1908, approximately 750 heteropoly compounds had been reported. However, the structure of polyoxometalates had remained a mystery for more than a century since their discovery. In 1933, Keggin solved the structure of the most important 12:1 type of heteropoly anions by a powder X-ray diffraction study of $H_3[PW_{12}O_{40}]\cdot 5H_2O$.[28] It is important to remember that there are hundreds of structures pertaining to POMs both isopoly and heteropoly. The most common structures are shown in Figure 1-1.

The Keggin structure (Figure 1-1a) is the first and best known polyoxometalate structural type. Keggin POMs overall exhibit virtual tetrahedral (T_d) symmetry, with a central XO_4 tetrahedral unit surrounded by 12 MO_6 octahedral units which are arranged into four groups of three edge sharing M_3O_{13} (M = W, Mo) units. Each of the four M_3O_{13} groups is linked to the central XO_4 unit and to each other by their corresponding edges. X is a main group element (P^V, Si^{IV}, Al^{III}, Ge^{IV}, etc.) or a transition metal ion (Fe^{III}, Co^{II}, Co^{III}, Cu^{I}, Cu^{II}, ect). Any POM with a general ratio of one heteroatom to twelve addenda atoms is labeled as 'Keggin' and those with a ration of 2:18 are labeled as 'Dawson' types (Figure 1-1c). The Keggin framework can undergo many electron-reduction processes without significantly deforming the framework.[29] Series of polytungstate anions $[XW_{12}O_{40}]^{n-}$ (X = P, Si, Fe, Co, or H_2; n= 3, 4, 5, 6, and 6 respectively) have been studied as sensitizers for the photoreduction of water and O_2. $[SiW_{12}O_{40}]^{4-}$ was the most efficient sensitizer for H_2 evolution in the presence of colloidal platinum. When $[SiW_{12}O_{40}]^{4-}$ undergoes several rapid one- and two-electron reversible reductions to give the familiar heteropoly blue anion, the produced heteropoly blue anion is very stable and can exist for long time in deaerated solution, so that the reduced 12-tungstosilicate with colloidal platinum can catalyze the reduction of water efficiently.[30]

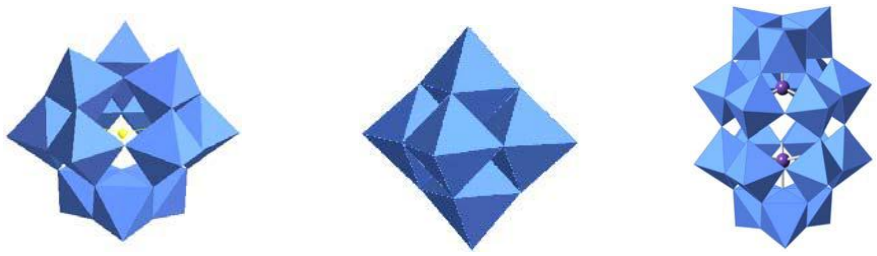

(a) **(b)** **(c)**

Figure 1. Polyhedral representation of a) Keggin, b) Lindqvist, c) Dawson POMs.[21,22]

The Lindqvist family of POMs have the general formula, $[M_6O_{19}]^{n-}$, (M = Nb, Ta, Mo, W).[31] Lindqvist POMs contain three distinct type of metal-oxygen bonds, as revealed through x-ray crystallography (Table 1-1). A central oxygen atom is bound to six metal atoms, with local octahedral symmetry. In figure 1-2, each metal atom is capped by terminal oxo ligand via a formal triple bond (one σ-bond and two π-bonds), and shares four bridging oxo ligands with adjacent metal atoms. These hexa-metalates have an idealized octahedral symmetry.[35] The Lindqvist anions $[M_6O_{19}]^{2-}$ (M= Mo, W) exhibit high point group symmetry and have been viewed as a model for an ideal oxide surface.[36]

Table 1. Selected bond lengths (Å) of some Lindqvist ($[M_6O_{19}]^{n-}$) isopolyanions.

Lindqvist POM	M-O (terminal)	M-O (bridging)	M-O (central)	Refs.
$[Mo_6O_{19}]^{2-}$	1.68	1.93	2.32	32
$[Ta_6O_{19}]^{8-}$	1.80	1.99	2.38	22
$[W_6O_{19}]^{2-}$	1.69	1.92	2.38	33

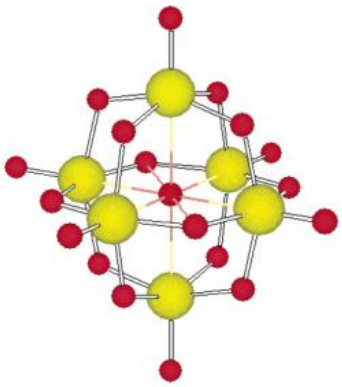

Figure 2. Ball and Stick Representation of the Lindqvist POM.

(Big/Yellow = Metal; Small/Red = Oxygen)[34]

POMs, with well-defined structures and properties, and with their size typically of a few nm, show similar properties to aggregates of various metal oxides. For example, like some metal oxides that can participate in catalytic processes as oxygen and multielectron relays, some polytungstate anions can sensitize the photochemical reduction of oxygen and water.[25a] In aqueous solution, $Na_6[H_2W_{12}O_{40}]$ can act as an electron carrier in the photoreduction of water by chloroplasts.[30a] Moreover, POMs have been studied for their photocatalytic properties in reduction of water due to their similarities in properties to nanonsized semiconductor materials such as TiO_2 and ZnO. The redox property of POMs is characterized by their ability to undergo stepwise, multielectron redox reactions, whilst their structure remains intact.[37] Thus, POMs have attracted significant attention as photocatalysts.

However, the metal ions in the oxidized polyoxometalates have d^0 electron configurations, the only absorption band which occurs in the UV-vis range of the electronic spectra is due to the oxygen−to−metal (O→M) ligand-to-metal charge transfer (LMCT).[38] In other words, POMs are predominantly ultraviolet absorbers and are not strongly activated by visible light, which presents a significant drawback in practical applications. Furthermore POMs can dissolve in a variety of solvents,[25b] so that POMs are difficult to be isolated and recycled by filtration. POMs can decompose even at mildly basic conditions.[21] As a consequence, it is necessary to combine these anions with visible photosensitizers based on simple ruthenium(II) polypyridyl complexes to form hybrid organic-inorganic solids. Hybrid compounds containing POMs have shown exciting electronic, optical, magnetic and catalytic properties, which make POMs attractive inorganic candidates.[3] When the new molecular hybrid materials are

synthesized by POMs and ruthenium polypyridyl complexes, they can be used as photo catalysts under visible light irradiation, in which ruthenium(II) polypyridyl complexes are expected to inject electrons to POMs through various interactions such as hydrogen bonding, electrostatic interactions and coordination bonds.

1.5 Combination of POMs and Ru Complexes

McCormac et al. synthesized the compound $[Ru(bpy)_3]_3[P_2W_{18}O_{62}]$ and investigated its electrochemistry both in aqueous solution and solid state.[39] Bond et al. showed the voltammetric, photo-physical and photo-electrochemical behaviors of the compounds $[Ru(bpy)_3]_2[S_2M_{18}O_{62}]$ (M = Mo, W).[40] Keyes et al. obtained three compounds, $[Ru(bpy)_3]_{3.5}[P_2W_{17}O_{61}(FeOH)]$, $[Ru(bpy)_3]_3[P_2W_{17}O_{61}(FeBr)]$ and $[Ru(bpy)_3]_5[P_2W_{17}O_{61}]$, and studied their photophysic properties.[41] Wang et al. reported two compounds, $[Ru(bpy)_3]$-$[PMo_{12}O_{40}]$ and $[Ru(bpy)_3]_2[S_2Mo_{18}O_{62}]$, which were used as the bifunctional electrocatalyst for the fabrication of the chemically bulk-modified carbon paste electrode.[42] Bi et al. synthesized the nanoparticles of $[Ru(bpy)_3]_2SiW_{12}O_{40}\cdot 2H_2O$ and applied them as electrochemiluminescence sensor.[43] However, all of the above compounds were characterized by elemental analysis, IR spectra and electrochemistry. To the best of our knowledge, there are only four reported on the structurally-characterized hybrid compounds $[Ru(2,2'\text{-}bpy)_3]_2[W_{10}O_{32}]\cdot 3dmso$,[44] $KNa[Ru(2,2'\text{-}bpy)_3]_2[H_2W_{12}O_{40}]\cdot 8H_2O$,[45] $K_6[Ru(pzc)_3]_2[SiW_{12}O_{40}]\cdot 12H_2O$,[45] $[Ru(bpy)_3][KPW_{12}O_{40}]$.[46]

Hybrid compounds containing polyoxometalates and ruthenium polypyridyl complexes can be isolated under routine synthetic reactions. For example, Wang et al. prepared $[Ru(bpy)_3]_2[W_{10}O_{32}]_3\cdot DMSO$. Tris-[2,2'-bipyridine]ruthenium(II) chloride

($[Ru(2,2'\text{-}bpy)_3]Cl_2 \cdot 6H_2O$) (0.2g) dissolved in 20 mL DMSO was added dropwise to a 30 mL acetonitrile solution of 2 g decatungstate $(NBu_4)_4W_{10}O_{32}$, stirring them 1 hour at 80^{o}C. The red solution was allowed to stand for six weeks and the red block crystal was obtained.[47] Bi et al. described four new organic-inorganic hybrid compounds which based on DMSO-coordinated heteropolytungstates as $[Ru(2,2'\text{-}bpy)_3]^{2+}$ salts{$[Ru(2,2'\text{-}bpy)_3]_2Na_2[Sb_2W_{22}(DMSO)_4O_{72}] \cdot 4DMSO \cdot 4H_2O$,{$[Ru(2,2'\text{-}bpy)_3]_2[Sb_2W_{20}Fe_2(DMSO)_8O_{68}] \cdot 9DMSO \cdot 12H_2O$, {$[Ru(2,2'\text{-}bpy)_3]_2Na_2[Bi_2W_{22}(DMSO)_4O_{72}] \cdot 4DMSO \cdot 4H_2O$, {$[Ru(2,2'\text{-}bpy)_3]_2[Bi_2W_{20}Fe_2(DMSO)_8O_{68}] \cdot 9DMSO \cdot 12H_2O$ and prepared them by routine synthetic reactions in the mixed solutions with DMSO/H_2O (1:1, v/v).[3] Bi et al also synthesized the novel hybrid nanoparticles, $[Ru(2,2'\text{-}bpy)_3]_2SiW_{12}O_{40} \cdot 2H_2O$. $[Ru(2,2'\text{-}bpy)_3]Cl_2 \cdot 6H_2O$ (0.2g) dissolved in 20 mL 0.1 M H_2SO_4 solutions, to which 30 mL 0.1 M H_2SO_4 solution containing 2 g 12-tungstosilicate ($H_4SiW_{12}O_{40}$) was added dropwise. The solution was stirred for 1 hour at room temperature. The $[Ru(2,2'\text{-}bpy)_3]_2SiW_{12}O_{40} \cdot 2H_2O$ sols were orange and separated by centrifugal machine for 5 min, and dispersed in alcohol by ultrasonication, and separated again. Finally, $[Ru(2,2'\text{-}bpy)_3]_2SiW_{12}O_{40} \cdot 2H_2O$ nanoparticles were obtained.[43] Routine synthetic method is a simple way to obtain hybrid solids and it requires less energy. It is simply mixing the two units into organic solvents or mixed solutions, and then stirring for a period of time or standing at room temperature for several days or weeks. After isolating and drying, the new hybrid solids can be collected.

1.6 Synthesis Method

The self-assembly of polyoxometalates and ruthenium polypyridine complexes into a hybrid solid will be carried out by hydrothermal reaction methods or room temperature solution approach.

Hydrothermal research was begun in the middle of the 19th century by geologists and was aimed at laboratory simulations of natural hydrothermal phenomena. In the 20th century, hydrothermal synthesis was clearly identified as an important technology for materials synthesis, predominantly in the fields of hydrometallurgy and single crystal growth. In recent years, this technique is being employed on a large scale to prepare piezoelectric, magnetic, optic, ceramic and a host of other materials both as single crystals and polycrystalline materials.[48] The hydrothermal method has several advantages over traditional solid state reactions. For instance, compounds which have elements with an unusual oxidation state may be synthesized by the hydrothermal method.[48] Another important advantage is that this method is useful for the synthesis of low temperature phases and metastable compounds.[48] Hydrothermal reactions do not require much time compared to traditional methods. Although a solid state reaction may be done in a few weeks, the hydrothermal reaction can be performed in a few days.

The term hydrothermal usually refers to any heterogeneous reaction in the presence of aqueous solvents or mineralizes under high pressure and temperature conditions in order to dissolve and recrystallize materials which are relatively insoluble under ordinary conditions.[48] According to Morey and Niggli, the components in the hydrothermal method are subjected to the action of water, at temperature generally above the critical temperature of water (~370^{o}C) in closed bombs, and therefore, under the

corresponding high pressures developed by such solutions.[50] Rabenau stated that hydrothermal synthesis is the heterogeneous reactions in aqueous media above 100^{o}C and 1 bar.[49] Roy defined that hydrothermal synthesis uses water as a catalyst and occasionally as a component of solid phases in the synthesis at elevated temperature (>100^{o}C) and pressure (greater than a few atmospheres).[51] Although the majority of scientists think of hydrothermal synthesis as taking place above 100^{o}C temperature and above 1 bar, there is no definite lower limit for temperature and pressure conditions.

Under hydrothermal conditions the reactants go into solution as complexes under the action of mineralizers or solvents. Water is the most important solvent for most ionic compounds. The properties of water under hydrothermal conditions are very different from water at standard conditions. It can dissolve nonionic covalent compounds such as insoluble oxides at high pressures and at temperatures above its boiling point at 1 bar pressure.[52] However, some compounds do not show high solubility for water even at supercritical temperature, and the size of the obtained crystals or minerals did not exceed thousandths or hundredth of a millimeter in all the early hydrothermal experiments. Therefore, in the 19th century the search for other suitable mineralizers began.[48] The function of mineralizer is in controlling the dissolution, nucleation and crystallization process under the action of temperature and pressure.[53] When used in small quantities, mineralizers function as catalysts which can speed up crystallization.[54] The mineralizer increases the solubility of the solute through the formation of soluble species which would not normally be present in the water. For example, the solubility of quartz in water at 400^{o}C and 2 kbar is too small to permit the recrystallization of quartz, in a temperature gradient, within a reasonable amount of time. However, with the addition

sodium hydroxide as a mineralizer, large quartz crystals may be grown.[55] Different mineralizers result in crystals of different sizes and shapes. Typical mineralizers are the hydroxides of alkali metals, (e.g. NaOH, KOH, LiOH), alkali salts of weak acids, (e.g. Na_2CO_3, Na_3BO_3, Na_2S), and the halides of alkali metals, (e.g. NaF, KF, LiF, NaCl, KCl, LiCl).[56]

Normally, hydrothermal reactions are carried out in PTFE (polytetrafluoroethylene)-lined acid digestion bombs (Figure 1-3). A typical hydrothermal procedure is as follows: The precursor substance is put at the bottom of the PTFE cup. The PTFE cup is filled to the desired degree with the solvent (water and mineralizer). This slurry is heated to the desired reaction temperature. At this temperature the starting materials react and/or transform, primarily through dissolution and precipitation, to the stable compound. After cooling the autoclave, the product is isolated by filtration and washed in order to obtain pure products.[57]

Figure 3. PTFE cup with cover, acid digestion bomb body, screw cap, pressure plate (upper), pressure plate (lower), corrosion and rupture discs, spring (from left to right).

1.7 Outline of Thesis

Chapter 1 introduces the background of this research including POMs, ruthenium complexes and the hydrothermal method.

Chapter 2 describes the synthesis methods and characterization techniques used in this research. Major chemicals used are also listed in this chapter.

Chapter 3 describes the synthesis, structures and characterization of the two polyoxometalate-photosensitizer hybrid materials $[Ru(2,2'\text{-bpy})_3]_2[SiW_{12}O_{40}]$ (**1**) and $[Ru(2,2'\text{-bpy})_2(CH_3CN)_2]_2[SiW_{12}O_{40}]$ (**2**).

Chapter 4 describes the synthesis, structures and properties of two novel cation radial salts containing $[Ru(2,2'\text{-bpy})_3]^{2+}$ and Lindqvist POMs, $[Ru(2,2'\text{-bpy})_3][W_6O_{19}]$ (**3**) and $[Ru(2,2'\text{-bpy})_3]_2[Mo_8O_{26}]\cdot 5H_2O$ (**4**).

Chapter 5 concludes the thesis and outlines future work.

CHAPTER 2

Experimental Methods

2.1 Synthesis Method

PTFE (polytetrafluoroethylene)-lined acid digestion bombs purchased from Parr Instrument Company (Illinois, USA) were used as reaction autoclaves. The maximum operating temperature is 250^{o}C and the maximum pressure is 1800 psi for autoclaves that are used in our experiments. When an aqueous solution is heated to 250^{o}C, it expands to fill a space approximately 25% larger than its volume at room temperature. If there is insufficient vapor space in the bomb to accommodate this expansion, the tremendous hydrostatic pressure which will be generated will destroy the bomb.[58] The bomb must never be completely filled as there must always be vapor space above the surface of the charge. The total volume of the charge must never exceed two thirds of the capacity of the cup when working with inorganic materials.[58] In all cases the size of the sample and the amount of oxidant used must be carefully controlled.

We used 23 mL and 45 mL Teflon lined autoclaves in our laboratory for hydrothermal syntheses (Figure 2-1). In this project, the reactants were mixed under ambient conditions and the acidity of the mixture is adjusted with acid or base. The reaction mixtures were first added to 3"×4" Teflon bags and then transferred to the Teflon cup. The Teflon cup was placed into a reaction autoclave, which was placed into an oven heated for desired reaction time at temperatures below 220^{o}C. The autoclave was then cooled to room temperature in the oven.

Figure 4. 23 mL (left) and 45 mL (right) autoclaves.

After cooling, the obtained product was washed several times with distilled water in order to remove the excess solvent from the crystals. The obtained single crystals were selected under Fisher Science Education Advanced Stereo Zoom Microscope for further analysis. The selected single crystal was mounted with epoxy on a glass fiber for analysis by single crystal X-ray diffractometry.

In this project, the synthesis of new hybrid solids was carried out by using room temperature solution method as well. The synthesis of the new solids started from preparing polyoxotungstate solution and ruthenium complexes solution. The polyoxotungstate solution and ruthenium complexes solution were added into a 27.25×70 mm vial with polyvinyl lined cap. The resulting solution was allowed to stand for several days before the crystalline hybrid solids were obtained. The obtained product was washed several times with acetonitrile and was dried at room temperature overnight.

2.2 Reagents

All chemicals were obtained from commercial sources and used without purification. No hazards were encountered in the experimental work reported.

Name	Formula	Company	Purity
2,2'-Bipyridine	$C_{10}H_8N_2$	Sigma-Aldrich	≥99%
*cis-Bis(*2,2'-bipyridine)dichloro-ruthenium(II) hydrate	$C_{20}H_{16}Cl_2N_4Ru$	Sigma-Aldrich	For R&D use only
Tri(2,2'-bipyridyl)dichloro-ruthenium(II) hexahydrate, powder	$C_{30}H_{24}C_{l2}N_6Ru$	Sigma-Aldrich	For R&D use only
Sodium metatungstate monohydrate	$3Na_2WO_4{\cdot}9WO_3{\cdot}H_2O$	Alfa Aesar	For R&D use only
Molybdic acid, MoO_3 85% min	$MoO_3{\cdot}H_2O$	Alfa Aesar	For R&D use only
Tungstosilicic acid hydrate	$H_4SiO_4{\cdot}12WO_3{\cdot}xH_2O$	Alfa Aesar	For R&D use only
Acetonitrile	C_2H_3N	Alfa Aesar	≥99%

2.3 Characterization Techniques

Several techniques are used in combination for complete characterization of new solid compounds, because there is not a single technique which is capable of providing complete characterization. The physical techniques which may be used to characterize solids are classified into three main categories: diffraction, microscopic and spectroscopic techniques. Furthermore, other techniques such as thermal analysis, and elemental analysis were also used.[59]

Powder X-ray Diffraction

New crystalline phases were identified by powder X-ray diffraction. Each crystalline solid has its own characteristic X-ray powder pattern (fingerprint) for its identification. When the new solid has been identified, the next stage is to determine its structure with single-crystal X-ray diffraction.

X-ray diffraction is a versatile analytical technique for examining crystalline solids, including ceramics, metals, electronic materials, geological materials, organic, and polymers. These materials may be powders, single crystals, multilayer thin films, sheets, fibers, or irregular shapes, depending on the desired measurement. X-ray diffractometers fall broadly into two classes: single-crystal and powder.[60] The operative equation in X-ray diffraction is the Bragg equation:

$$n\lambda = 2d \sin\theta$$

where n is the order of a reflection (n = 1, 2, 3 . . .), λ the wavelength, d the distance between parallel lattice planes, and θ the angle between the incident beam and a lattice plane. In general, the more symmetrical the material, the fewer peaks in its diffraction pattern. The diffracted intensities associated with those peaks are determined by the type and arrangement of atoms within the crystal lattice.[61]

Powder X-ray diffraction is a non-destructive and rapid analytical technique widely applied for the characterization of crystalline materials.[62] Powder diffractometers are routinely used for phase identification and quantitative phase analysis but can be configured for many applications, which include variable-temperature studies, texture and stress analysis, grazing incidence diffraction, and reflectometry.[60]

X-ray diffractometers consist of three basic elements: an X-ray tube, a sample holder, and an X-ray detector (Figure 2-2). In X-ray powder diffractometry, X-rays are generated within a cathode ray tube that is under vacuum by heating a filament to product electrons. A high voltage is applied within the tube. This high voltage accelerates the electrons, which then hit a target, commonly made by copper. When electrons have

sufficient energy to dislodge inner shell electrons of the target material, characteristic X-ray spectra are produced.[63]

A powdered sample is placed on a holder, and then the sample is illuminated with x-rays of a fixed wavelength. As the sample and detector are rotated, the intensity of the reflected X-rays is recorded (Figure 2-2). When the geometry of the incident X-rays impinging the sample satisfies the Bragg Equation ($n\lambda = 2d\sin\theta$), constructive interference occurs and a peak in intensity occurs. This law relates the wavelength of electromagnetic radiation to the diffraction angle and the lattice spacing in a crystalline sample. These diffracted X-rays are then detected, processed and counted. By scanning the sample through a range of 2θ angles, all possible diffraction directions of the lattice should be attained due to the random orientation of the powdered material. Conversion of the diffraction peaks to *d*-spacings allows identification of the mineral because each mineral has a set of unique *d*-spacings. Typically, this is achieved by comparison of d-spacings with standard reference patterns. In figure 2-3, it is an example of an X-ray powder diffractogram which was produced during an X-ray scan.[64] The positions of the peaks where the X-ray beam has been diffracted by the crystal lattice are directly related to the dimensions of the unit cell. The intensities are related to the contents of the unit cell. The set of *d*-spacings (the distance between adjacent planes of atoms), which represent the unique "fingerprint" of the mineral, can easily be calculated from the 2θ values shown.[65] The angle and the d-spacings are related by Bragg Equation, as described above.

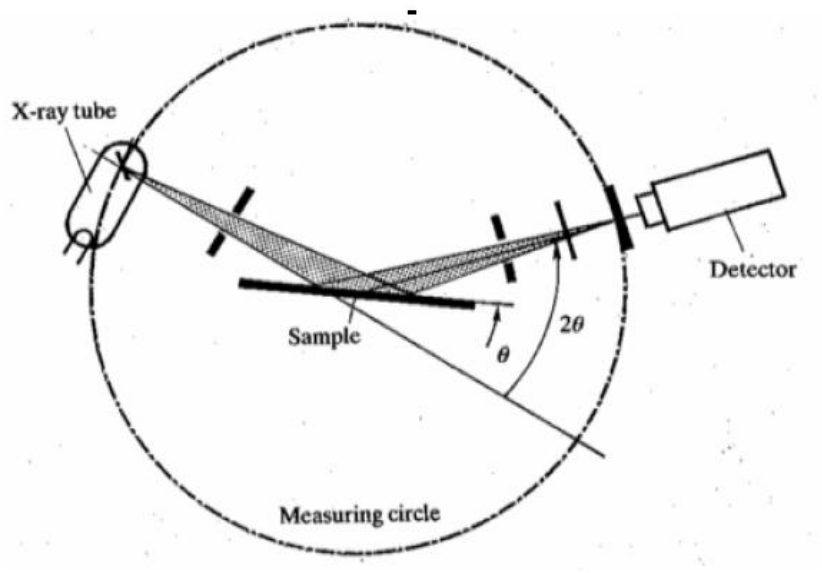

Figure 5. Diagram of a powder diffractometer.[63]

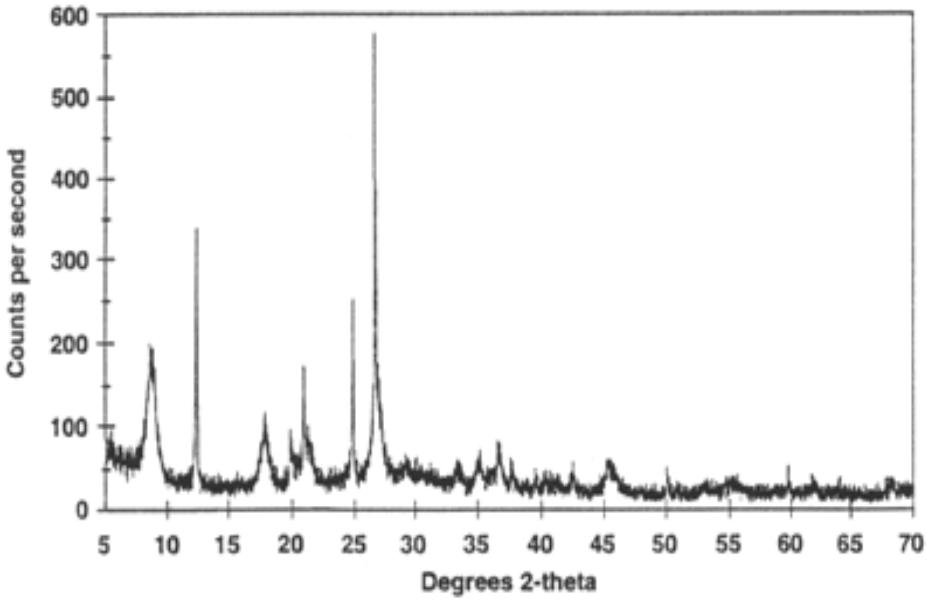

Figure 6. Diffractogram of an X-ray powder.[64]

There is a regularly updated library of power diffraction patterns which is known as the JCPDS – Joint Committee for Powder Diffraction Standards – file (formerly known as the ASTM File).[63] The file contains over 35000 inorganic substances.

In our research X-ray powder diffraction patterns were obtained by using a MiniFlexII Desk Top X-ray diffractometer. Samples were placed on a zero background silicon sample holder. Data were collected by using Cu Kα (λ = 1.5418 Å) radiation at setting of 30 kV and 15 mA. The scan rate was 0.1°/sec and the data was collected 2θ values of 5° to 70°.

Single Crystal X-ray Diffraction

Single-crystal X-ray diffraction is a non-destructive analytical technique which provides detailed information about the internal lattice of crystalline substances, including unit cell dimensions, bond-lengths, bond-angles, and details of site-ordering.[66] Single-crystal diffractometers are most often used to determine the structures of new solid materials.[60]

A single crystal is made up of a large number of atoms which are arranged in a precisely regular way repeated in all directions to give a highly ordered structure. The basic building in a crystal is the unit cell. A crystal is made up of millions of identical unit cells arranged in a three dimensional crystal lattice. Each crystalline substance has a unique set of lattice constants (a, b, c, α, β, γ) which define the size and shape of the unit cell (Figure 2-4). When a beam of parallel monochromatic X-rays of approximately 1 Å wavelength strikes a single crystal, the crystal acts as a three dimensional diffraction grating and produces an X-ray diffraction pattern (Figure 2-5). This diffraction consists of a three-dimensional array of reflections that satisfy the condition of Bragg's law.

Therefore, from a single crystal the position and intensity of the diffraction peaks can be measured accurately and from this data the substance may be classified into one of seven crystal systems (i.e., triclinic, monoclinic, orthorhombic, tetragonal, cubic, trigonal or hexagonal). Finally, each substance may be further classified as belonging to one of 230 three dimensional space groups. The lattice constants, crystal system, and space group are important physical constants for crystalline substances and may be used in conjunction with other physical measurements to explain the properties of solid-state materials.[67]

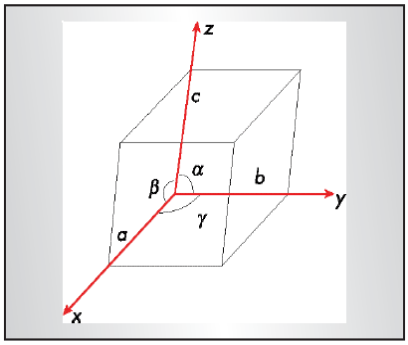

Figure 7. Diagram of Unite Cell: the reference axes x, y, z are right-handed, the length of the unit-cell edge parallel to each reference axis is *a*, *b*, *c*, respectively. And the interaxial angles are *α, β, γ*, respectively.[67]

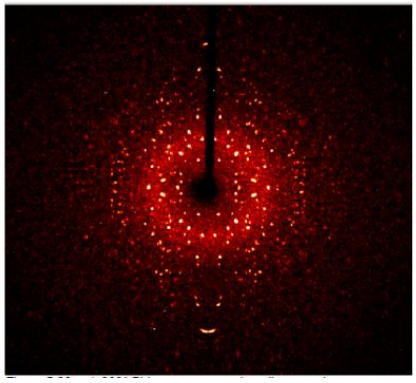

Figure 8. An example of an X-ray diffraction pattern produced by a single crystal.[68]

Samples for single-crystal diffraction should be selected from unfractured, transparent, faces, and looks single. This can be determined by viewing the samples under a microscope. Samples should be between 30 and 300 μm. To minimize absorption affects, spherical crystals are preferred. Samples are mounted on the tip of a thin glass fiber using super glue. This fiber is attached to a brass mounting pin, usually by the use of modeling clay, and the pin is then inserted into the goniometer head (Figure 2-6).[68]

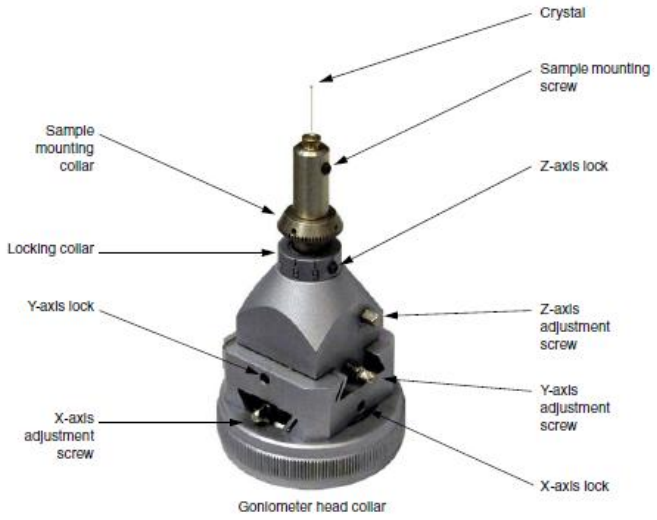

Figure 9. Image of goniometer head.[68]

The goniometer head and sample are then affixed to the diffractometer (Figure 2-7). Samples can be centered by viewing the sample under an attached microscope or video camera and adjusting the X, Y, and Z directions until the sample is centered under the cross hair for all crystal orientations (Figure 2-8). Once the crystal is centered, an automatic collection routine can then be used to collect data. A complete data collection may require anywhere between 6-24 hour, depending on the specimen and the diffractometer.[66]

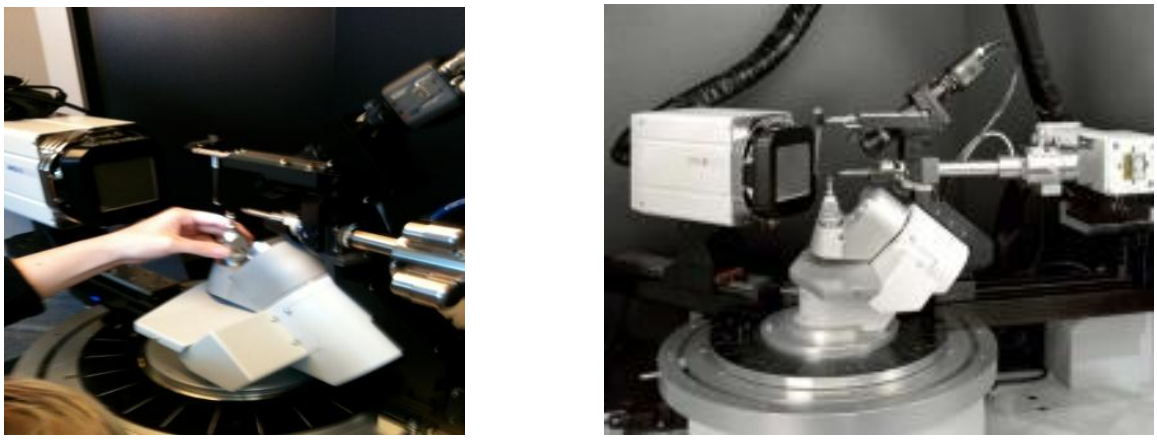

Figure 10. Images of single-crystal X-ray Diffraction.

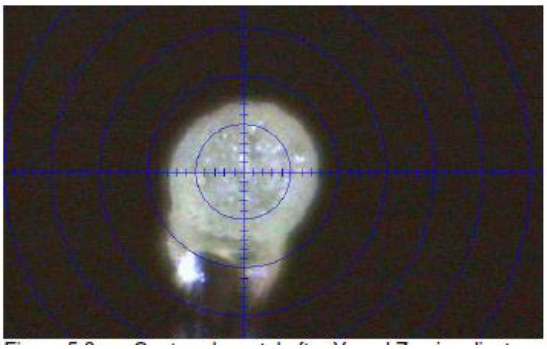

Figure 11. Image of the cross hair.[68]

The software used in solving crystal structures is the SHELXTL program suite. The different programs in this suite, including XPREP, XP and SHELXL, allow for the initial solution of the phase problem, imaging of the crystal and refinement of the structure.[69]

In our research single crystal X-ray diffraction data were collected on a KAPPA APEX II diffractometer with APEX II detector (Figure 2-9). Graphite-monochromated molybdenum radiation Mo Kα (λ=0.71073 Å) from a sealed tube generator was used. Raw data were integrated, scaled, merged and corrected for Lorentz-polarization effects using the HKL-SMN package.[70] The structure was solved by direct methods (SHELXS97) and refined by the full-matrix-block least-squares method on F^2.[71] All non-

hydrogen atoms were refined with anisotropic displacement parameters. Atomic scattering factors were taken from the International Tables for Crystallography.[72]

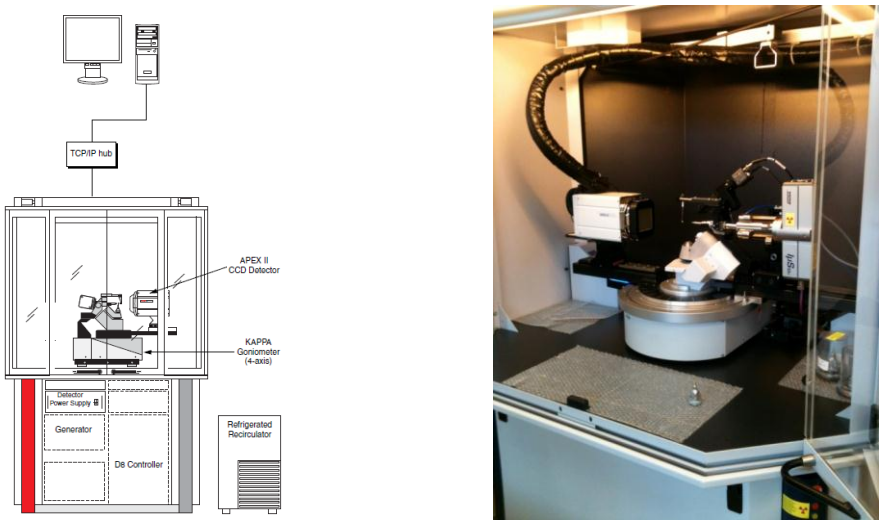

a b

Figure 12. a) Diagram of KAPPA APEX II system; b) Image of KAPPA APEX II diffractometer with APEX II detector.

Ultraviolet-Visible Spectrophotometer

The ultraviolet-visible (UV−vis) spectroscopy was used to determine the electronic structure of substances. The ultraviolet region of the spectrum is generally considered to range from 200 to 400 nm and the visible region from 400 to 800 nm. The UV−vis spectrophotometer is widely used for identification of many types of inorganic and organic molecules, and ions; and quantitative determination of many biological, organic; and inorganic species. Any transparent solid, liquid, or gaseous sample can be used in spectroscopic analysis. Opaque solids and liquids can be measured with reflectance or photoacoustic techniques. Turbid samples can sometimes be accommodated with derivative techniques.[60] In our research the UV−vis diffusion reflectance spectra of the hybrid materials were recorded on a Varian Cary 100 UV-VIS

spectrophotometer equipped with the DRA-CA-30 diffuse reflectance accessory. The UV−vis spectra provided information on the electronic structure of the synthesized materials, especially the metal to ligand charge transfer band for ruthenium polypyridyl complexes.

Infrared (IR) Spectroscopy

Infrared (IR) spectroscopy is the absorption measurement of different IR frequencies by a sample positioned in the path of an IR beam. The infrared region of the electromagnetic spectrum is found from 400 cm^{-1} to 4000 cm^{-1}. Infrared spectroscopy concerns the vibrational motion of molecules. The main goal of IR spectroscopic analysis is to determine the chemical functional groups in the sample. Different functional groups absorb characteristic frequencies of IR radiation. IR spectroscopy can accept a wide range of sample types such as gases, liquids, and solids by using various sampling accessories. Thus, IR spectroscopy is an important and popular tool for structural explanation and compound identification.[60,73]

IR spectra are obtained by detecting changes in transmittance (or absorption) intensity as a function of frequency or wavenumber (cm^{-1}). Most commercial instruments separate and measure IR radiation using dispersive spectrometers or Fourier transform spectrometers (FTIR). A FTIR spectrometer offers superior speed and sensitivity, so recently it has replaced dispersive instruments for most applications. It is possible to obtain an IR spectrum from samples in many different forms, such as liquid, solid, and gas. However, many materials are opaque to IR radiation and must be dissolved or diluted in a transparent matrix in order to obtain spectra. For example, pellets are used for solid samples. The sample (0.5 to 1.0 mg) is finely ground and intimately mixed with

approximately 100 mg of dry potassium bromide (KBr) or other alkali halide powder. Grinding and mixing can be done with an agate mortar and pestle. The mixture is then pressed into a transparent disk in an evacuable die at sufficiently high pressure. Suitable KBr disks or pellets can often be made using a simpler device such as a Mini-Press. To minimize band distortion due to scattering of radiation, the sample should be ground to particles of 2 μm or less in size. The IR spectra produced by the pellet technique often exhibit bands at 3450 cm^{-1} and 1640 cm^{-1} due to absorbed moisture.[60]

In our research the infrared spectra were recorded from 400 to 4000 cm^{-1} on a Perkin-Elmer Spectrum One FTIR spectrometer using KBr pellets.

Fluorescence Spectroscopy

Fluorescence spectroscopy is a type of electromagnetic spectroscopy which measures the intensity of photoluminescence to permit the quantitative determination of a variety of important inorganic and organic species in trace amounts. It is an important investigational tool in many areas of analytical science, due to its extremely high sensitivity and selectivity.[60,73,74] Photoluminescence is a type of optical spectroscopy in which a molecule is promoted to an electronically excited state by absorption of photons. The excited molecule then decays back to the ground state, or to a lower-lying excited electronic state, by emission of light. The emitted light is detected. Photoluminescence processes are subdivided into fluorescence and phosphorescence.[3] Fluorescence differs from phosphorescence in that the electronic energy transitions responsible for fluorescence do not involve a change in electron spin. Because of this, the excited states involved in fluorescence are short-lived ($<10^{-5}$s). In contrast, a change in electron spin

accompanies phosphorescence, and the lifetimes of the excited states are much longer, often on the order of seconds or even minutes.[73]

Almost any solid, liquid, or gaseous sample can be analyzed, although solid samples may require a special sample compartment. Highly turbid liquid samples may cause difficulty.[3] The most intense and the most useful fluorescence is found in compounds containing aromatic functional groups with low-energy $\pi \rightarrow \pi^*$ transitions because such excited states exhibit relatively short average lifetimes. Compounds containing aliphatic and alicyclic carbonyl structures or highly conjugated double-bond structures may also exhibit fluorescence, but the number of these is smaller than the number in the aromatic systems.[73]

In our research a PerkinElmer L55 Luminescence Spectrometer was used. The possible electronic communication occurred between the polyoxometalates and the sensitizers ruthenium polypyridine complexes were examined using fluorescence spectra.

Thermogravimetric Analysis (TGA)

Thermogravimetric analysis is an essential laboratory tool used for material characterization. In thermogravimetric analysis the mass of a sample is monitored continuously as a function of temperature or time as the sample specimen is subjected to a controlled temperature program in a controlled atmosphere. A plot of mass or mass percentage as a function of time is called a thermogram or a thermal decomposition curve.[73]

TGA is used to determine the loss in mass at particular temperatures, so the information provided is quantitative. It is limited to decomposition and oxidation reactions and to such physical processes as vaporization, sublimation, and desorption.

The temperature range for thermogravimetric analysis is from ambient to 1500^{o}C. The heating and cooling rates may be selected from somewhat greater than zero to as high as 200^{o}C/min. A sample purge gas controls the sample environment. This gas may be inert or a reactive gas that flows over the sample and exits through an exhaust. Nitrogen or argon is usually used to prevent oxidation of the sample.[73]

In our research the thermogravimetric data were collected on a TA Q5000 TGA instrument. For thermogravimetric analysis 10 to 25 mg powder samples were placed in a sample pan. Temperature program is heat from room temperature to 700^{o}C at 10^{o}C/minute. The analyses were done under air atmosphere with a purge rate of 40 mL/minute.

CHAPTER 3

Keggin Polyoxometalate–Photosensitizer Hybrid Materials

ABSTRACT. Two hybrid materials $[Ru(2,2'\text{-}bpy)_3]_2[SiW_{12}O_{40}]$ (**1**) and $[Ru(2,2'\text{-}bpy)_2(CH_3CN)_2]_2[SiW_{12}O_{40}]$ (**2**) were synthesized using ruthenium polypyridyl complex ($[Ru(2,2'\text{-}bpy)_3]^{2+}$, or $[Ru(2,2'\text{-}bpy)_2(CH_3CN)_2]_2]^{2+}$, 2,2'-bpy = 2,2'-bipyridine) and a Keggin polyoxometalate $[SiW_{12}O_{40}]^{4-}$ as building unites. X-ray crystallographic study of these two hybrid solids show that the polyoxoanions $[SiW_{12}O_{40}]^{4-}$ are associated with the $[Ru(bpy)_3]^{2+}$ or $[Ru(2,2'\text{-}bpy)_2(CH_3CN)_2]^{2+}$ counter ions by Coulombic forces and hydrogen bond interactions. The molecular complexes are further connected and form three-dimensional frameworks through C-H···O_{POM} and other weak interactions. These two compounds were further characterized by C−H−N elemental analyses, FT-IR, UV-Vis, luminescent spectra, and thermogravimetric analysis. Significantly, these combined spectroscopic studies show that these polyoxometalate-dye hybrids have strong electronic interactions between the cationic dye and polyanion units.

3.1 Introduction

In recent years, much work has been done on the synthesis of hybrid materials containing POMs and tris-(2,2'-bipyridine) ruthenium(II) complexes.[39-43] However, to the best of our knowledge, there are only four reported on the structurally-characterized hybrid compounds.[44-46] The fundamental structural study on the single-phase crystalline hybrid solid materials containing both ruthenium complexes and POMs remains particularly challenging. Nevertheless, the potential photo-physical,[40] electrochemiluminescen,[43] and bifunctional electrocatalytic properties[42] of such species are a strong motivation to undergo this kind of research. In this chapter, the synthesis and characterization of two hybrid POM-dye compounds, $[Ru(2,2'\text{-}bpy)_3]_2[SiW_{12}O_{40}]$ (**1**) and $[Ru(2,2'\text{-}bpy)_2(CH_3CN)_2]_2[SiW_{12}O_{40}]$ (**2**) are described. X-ray crystallographic study of two hybrid solids showed that the polyanions $[SiW_{12}O_{40}]^{4-}$ are associated with the ruthenium complex counterions by Coulombic forces and hydrogen bond interactions.

3.2 Experimental

3.2.1 Syntheses

The reactions were carried out under hydrothermal conditions using 3"×4" Teflon bags in Teflon-lined stainless steel autoclave reactors.

$[Ru(2,2'\text{-}bpy)_3]_2[SiW_{12}O_{40}]$ (**1**) was synthesized hydrothermally from a mixture of tri-(2,2'-bipyridyl) dichloro-ruthenium(II) hexahydrate powder ($[Ru(2,2'\text{-}bpy)_3]Cl_2{\cdot}6H_2O$, 0.020 g), tungstosilicic acid hydrate ($H_4SiO_4{\cdot}12WO_3{\cdot}xH_2O$, 0.180 g), and deionized water (2.0 mL). The pH of the resulting mixture was adjusted with 0.5 mL of 1.0 M H_2SO_4 to approximately 2. The reaction mixtures were transferred to a Teflon bag, sealed and placed in a 45 mL reaction vessel, and heated in an oven to 200^{o}C for 72

hours. After the autoclave was cooled to room temperature naturally, the red crystals of **1** were filtered, washed with deionized water, and dried in air (yield based on Ru: 53%) (Figure 3-1). Elemental analysis: *calcd.* For $C_{60}H_{48}N_{12}O_{40}Ru_2SiW_{12}$: C, 17.95; H, 1.21; N, 4.19; *found*: C, 16.85; H, 1.03; N, 3.73%. FT-IR spectrum (KBr, cm^{-1}): 3526(broad), 3078(s), 1635(s), 1603(s), 1464(s), 1447(s), 1429(s)1012(s), 970(s), 921(s), 879(s), 794(s), 761(s). UV-visible (powder, λ_{max}/nm): 445.

$[Ru(2,2'\text{-}bpy)_2(CH_3CN)_2]_2[SiW_{12}O_{40}]$ (**2**) has been synthesized by routine synthetic reaction in mixed solvent of acetonitrile and water. Cis-bis (2,2'-bipyridine) dichlororuthenium(II) hydrate (0.5×10^{-3} M, 4.0 mL) and acetonitrile 6.0 mL were placed into a 27.25×70 mm vial (solution #1). $H_4SiO_4\cdot12WO_3\cdot xH_2O$ (0.5×10^{-3} M, 4.0 mL) and acetonitrile 6.0 mL were placed into another 27.25×70 mm vial (solution #2). Solution #1 (6.0 mL) and solution #2 (6.0 mL) were mixed into another 27.25×70 mm vial and then added 2.0 mL deionized water. The yellow solution was allowed to stand for three weeks at room temperature. The flake shape yellow crystals of **2** were filtered, washed with acetonitrile, and dried in air (yield based on Ru: 93.8%) (Figure 3-1).Elemental analysis: *calcd.* For $C_{48}H_{44}N_{12}O_{40}Ru_2SiW_{12}$: C, 14.92; H, 1.15; N, 4.35; *found*: C, 14.97; H, 1.41; N, 4.30%. IR (KBr pellet, cm^{-1}): 3568(broad), 1624(s), 1605(s), 1466(s), 1447(s), 1427(s), 1013(s), 970(s), 921(s), 793(s). UV-visible (powder, λ_{max}/nm): 413.

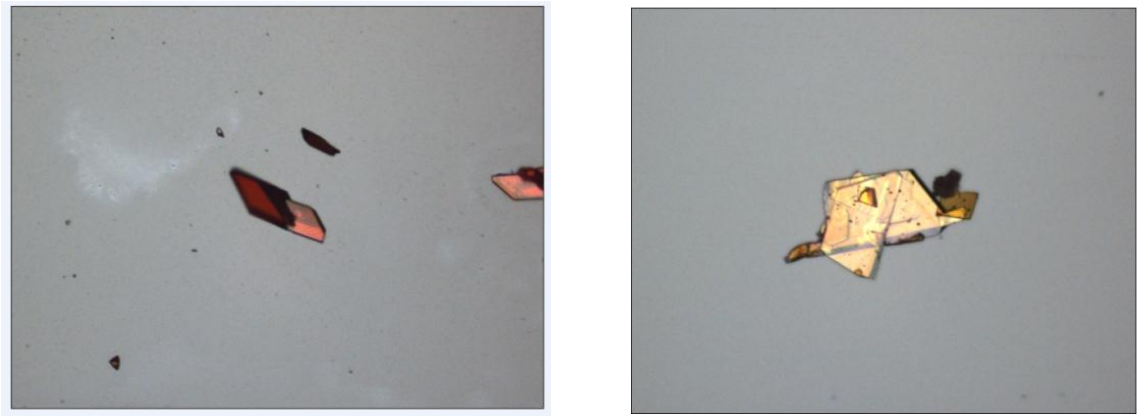

a b

Figure 13. (a) Stereomicroscope image of compound **1** (b) Stereomicroscope image of compound **2.**

3.2.2 X-ray Crystallography

X-ray diffraction data for compounds **1** and **2** were collected on a Bruker Kappa Apex II CCD diffractometer with graphite monochromated Mo *K*α radiation (λ = 0.71073Å) at 293(2) K. Crystal data and relevant details of the structure determinations are summarized in Table 3-1 and selected geometrical parameters are given in Table 3-2.

3.3 Results and Discussions

Compound **1** was synthesized using the hydrothermal method. The use of cluster compounds as starting materials is straight forward and the synthesis is easy to control. As expected, control of the pH of the reaction mixtures is critical for the crystallization of compound **1**. It can be crystallized in a narrow pH at around 2 and in a temperature range of 190-225^{o}C. Compound **2** was synthesized in one-step reaction by simply mixing solutions of the reactants. The resulting flake shape yellow crystals could be purified by washing with acetonitrile to remove the excess starting materials.

Table 2. Crystallographic parameters and refinement details for compounds **1** and **2**.

	1	**2**
Formula	$C_{60}H_{48}N_{12}O_{40}Ru_2SiW_{12}$	$C_{48}H_{44}N_{12}O_{40}Ru_2SiW_{12}$
Mol. wt.	4013.51	3865.35
Crystal system	Triclinic	Monoclinic
Space group	*P*–1 (2)	*C*2/*c* (15)
a (Å)	12.1024(3)	16.9988(8)
b(Å)	13.2906(4)	26.5340(14)
c(Å)	13.6920(4)	19.1481(10)
α(°)	70.071(2)	90
β(°)	86.868(2)	96.376(2)
γ(°)	84.492(2)	90
V($Å^3$)	2060.32(10)	8583.3(8)
Z	1	4
ρ (g/cm^3)	3.286	2.651
μ (mm^{-1})	17.141	16.260
Wavelength(Å)	0.71073	0.71073
Temperature(K)	296(2)	293(2)
Reflections collected/unique [R_{int}]	30512/5782[0.0480]	135315/7451[0.0635]
Goodness-of-fit(F^2)	1.140	1.095
Final R indices [$I > 2\sigma(I)$]	R_1= 0.0690, wR_2= 0.1626	R_1= 0.0452, wR_2= 0.1017
R indices (all data)	R_1= 0.0871, wR_2= 0.1724	R_1= 0.0711, wR_2= 0.1123

Table 3. Selected interatomic distances (Å) in compounds **1** and **2.**

Compound**1**		Compound**2**	
W–O_t	1.626(5)-1.664(1)	1.662-1.676(1)	
W–$O_{\mu 2}$	1.767(8)-1.971(6)	1.860-1.916(1)	
W–$O_{\mu 4}$	2.191(5)-2.586(6)	2.324-2.457(1)	
Si–O	1.464(7)-1.766(5)	1.561-1.671(1)	
Ru(1)–N(1)	2.040(4)	Ru(1)–N(4)	2.020(1)
Ru(1)–N(2)	2.040(4)	Ru(1)–N(13)	2.060(1)
Ru(1)–N(3)	2.071(8)	Ru(1)–N(20)	2.054(1)
Ru(1)–N(4)	2.072(3)	Ru(1)–N(21)	2.023(1)
Ru(1)–N(5)	2.055(2)		
Ru(1)–N(6)	2.039(1)	Ru(1)–N(11)	2.042(1)
		Ru(1)–N(34)	2.013(1)

3.3.1 Crystal Structure

Crystal structure of compound 1. Compound **1** crystallizes in the triclinic space group *P*-1. The structure of **1** consists of Keggin cluster anion $[SiW_{12}O_{40}]^{4-}$ and charge balancing cation $[Ru(2,2'\text{-bpy})_3]^{2+}$. At the center of the $[SiW_{12}O_{40}]^{4-}$ anion, the SiO_4 tetrahedron is disordered over two positions related by an inversion center at the site of Si atom (Si–O distances are in the range of 1.46(1)–1.77(1) Å). The classic $[SiW_{12}O_{40}]^{4-}$ Keggin cluster ion consists of twelve WO_6 octahedra with the three types of W−O bond lengths in normal range.[28] As usual, the W–O bond lengths decrease with the decreasing coordination number of the oxygen atom, with values averaging 2.389(2) Å for four-coordination ($O_{\mu 4}$), 1.869(7) Å for two-coordination ($O_{\mu 2}$) and 1.644(4) Å for the terminal oxygen atoms (O_t) (see Table 3-2). Bond valence sum calculations indicate all W atoms have the oxidation 6+.

Even though there are no "classical hydrogen bonds" between the $[Ru(2,2'\text{-bpy})_3]^{2+}$ cations and the Keggin ion $[SiW_{12}O_{40}]^{4-}$ in **1,** there are several CH···O contacts in the range 2.28–2.60 Å between these units (Table 3-3). These interactions involve both terminal and bridged oxo groups of Keggin ions. Each $[SiW_{12}O_{40}]^{4-}$ anion is hydrogen bonded to eight $[Ru(2,2'\text{-bpy})_3]^{2+}$ cations, and in turn each $[Ru(2,2'\text{-bpy})_3]^{2+}$ cation is hydrogen bonded to four $[SiW_{12}O_{40}]^{4-}$ anions to form a three-dimensional network (Figure 3-2).

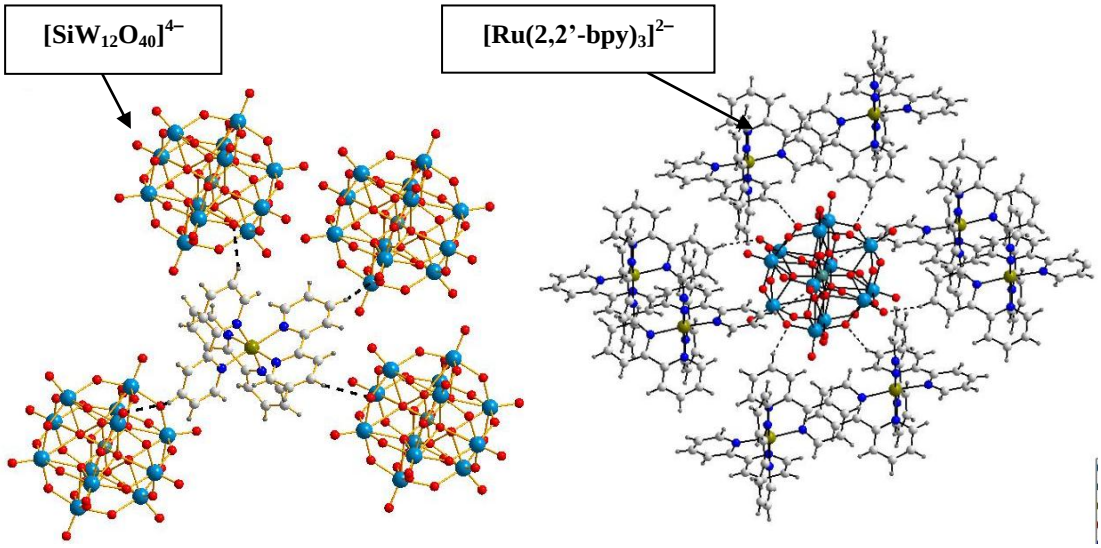

Figure 14. The $[Ru(2,2'\text{-}bpy)_3]^{2+}$ cation linked to$[SiW_{12}O_{40}]^{4-}$ anions through hydrogen bonding.

Table 4. Atomic distance (Å) and angles (^{o}) of $O_{POM}\cdots H_{pyr}$ interactions in the crystal structure of compound **1**.

Donor---H···Acceptor	d(D---H)	d(H····A)	d(D···A)	∠DHA
C(9)---H(9)···O(2)	0.94	2.60	3.34(5)	137
C(24)---H(24)···O(5)	0.93	2.28	3.19(5)	165
C(27)---H(27)···O(22)	0.93	2.41	3.26(5)	153
C(31)---H(31)···O(12)	0.93	2.53	3.38(7)	153

Crystal structure of compound 2. The single-crystal structure analysis of **2** reveals that it contains $[Ru(2,2'\text{-}bpy)_2(CH_3CN)_2]^{2+}$ cationic complex and Keggin ion $[SiW_{12}O_{40}]^{4-}$. Compound **2** has the same Keggin cluster ion $[SiW_{12}O_{40}]^{4-}$ as compound **1**. An interesting feature of compound **2** is that it contains an cationic Ru complex $[Ru(2,2'\text{-}bpy)_2(CH_3CN)_2]^{2+}$ (Figure 3-3). In this complex, the Ru(II) ion coordinates to two 2,2'-bipyridine ligands and two acetonitrile ligands. Bond length for Ru-N is in the range of 2.013(1)-2.060(1) Å. The Ru-N bond lengths are shorter than those in compound **1**. The

Ru-Ru distance of adjacent $[Ru(2,2'\text{-}bpy)_2(CH_3CN)_2]^{2+}$ units within a column is of 9.6911(3)Å.

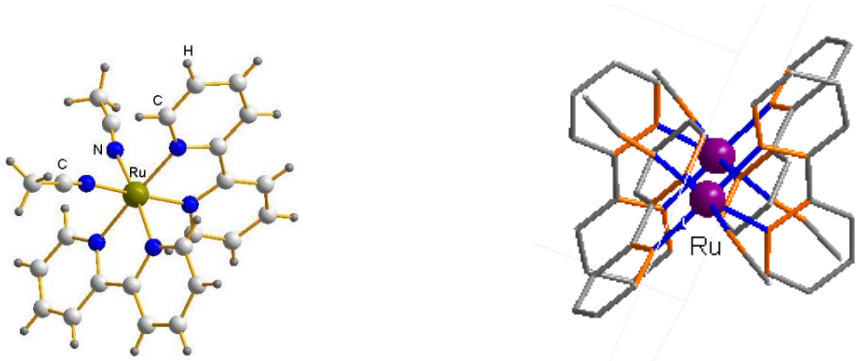

Figure 15. The complex ion $[Ru(2,2'\text{-}bpy)_2(CH_3CN)_2]^{2+}$ in compound **2**.

There are extensive C–H···O_{POM} hydrogen bonds between $[Ru(2,2'\text{-}bpy)_2(CH_3CN)_2]^{2+}$ and $[SiW_{12}O_{40}]^{4-}$ in **2**. Some of the CH···O interactions are listed in Table 3-4. These interactions involve terminal oxo groups of Keggin ions. Each $[SiW_{12}O_{40}]^{4-}$ anion is hydrogen bonded to four $[Ru(2,2'\text{-}bpy)_2(CH_3CN)_2]^{2+}$ cations, and in turn each $[Ru(2,2'\text{-}bpy)_2(CH_3CN)_2]^{2+}$ cations hydrogen bonded to two $[SiW_{12}O_{40}]^{4-}$anions to form a three-dimensional network (Figure 3-4). The hydrogen bonds among 2,2'-bipyridine, acetonitrile and $[SiW_{12}O_{40}]^{4-}$ are relatively weak, with H···O contact in the range of 2.45–2.60 Å.

Table 5. Atomic distance (Å) and angles (°) of O_{POM}···H_{pyr} interactions in the crystal structure of compound **2**.

Donor---H···Acceptor	d(D---H)	d(H····A)	d(D···A)	∠DHA
C(6A)---H(6A)···O(12)	0.93	2.60	3.31(9)	135
C(7A)---H(7A)···O(10)	0.93	2.45	3.02(8)	120
C(10B)---H(10)···O(9)	0.93	2.55	3.34(2)	143
C(17B)---H(17B)···O(6)	0.96	2.54	3.23(7)	130
C(17B)---H(17C)···O(8)	0.96	2.57	3.44(7)	152
C(19)---H(19)···O(1)	0.93	2.58	3.39(6)	146
C(25)---H(25)···O(3)	0.93	2.59	3.42(9)	150
C(26)---H(26)···O(4)	0.93	2.54	3.18(9)	127
C(37)---H(37)···N(34)	0.93	2.49	3.03(2)	118

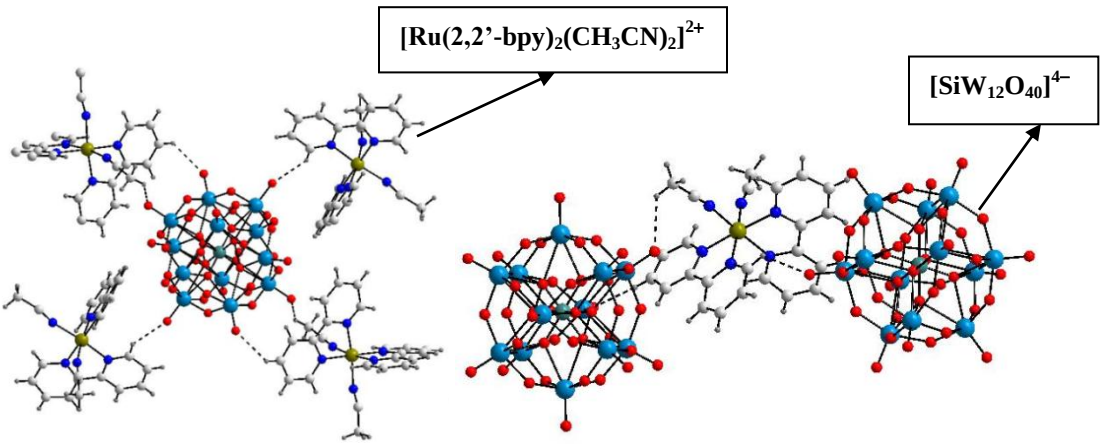

Figure 16. The $[Ru(2,2'\text{-}bpy)_2(CH_3CN)_2]^{2+}$cation linked to$[SiW_{12}O_{40}]^{4-}$ anions through hydrogen bonding.

The phase purity of compounds **1** and **2** were confirmed by comparing the powder X-ray diffraction (PXRD) patterns of the pristine sample and the simulated pattern from the crystal structure. Compounds **1** and **2** were pure products based on the agreement of their PXRD diffraction patterns and the simulated patterns (Figure 3-5).

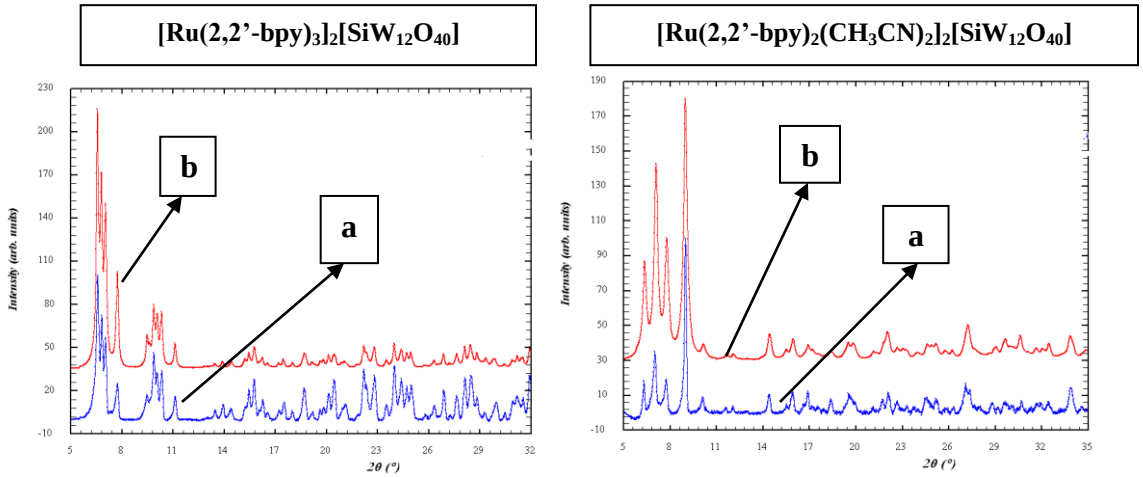

Figure 17. The powder X-ray diffraction patterns (blue line, a) and the simulated patterns (red line, b) of compounds **1** and **2**.

3.3.2 UV-vis Diffuse Reflectance Spectra

Figure 3-6 shows the UV-vis diffuse reflectance spectra on solid samples of compound **1** and $[Ru(2,2'\text{-bpy})_3]Cl_2\cdot 6H_2O$. The optical absorption spectrum of compound **1** was characterized by a broad band in the visible domain around 445 nm and a band peaking at 270 nm. The visible absorption band is attributed to a metal-to-ligand charge transfer (MLCT) transition in which an electron located in a metal-based d orbital is promoted into a ligand-centered π* orbital.[12b,75] The UV absorption band corresponds to a ligand-centered π–π* transition of 2,2'-bpy ligand, which is overlapped with the band of ligand-to-metal charge-transfer (LMCT) transitions for W(VI) (O→W).[76] The λ_{max}(445 nm) of MLCT band of compound **1** shows a red shift in comparison with $[Ru(2,2'\text{-bpy})_3]Cl_2\cdot 6H_2O$ (λ_{max}= 424 nm). The λ_{max} (270 nm) of UV absorption band of complex **1** shows a blue shift in comparison with $[Ru(2,2'\text{-bpy})_3]Cl_2\cdot 6H_2O$ (λ_{max}= 290 nm). These changes of charge transfer transitions in compound **1** indicate electronic communication occurred between the polyoxometalates and the sensitizers.

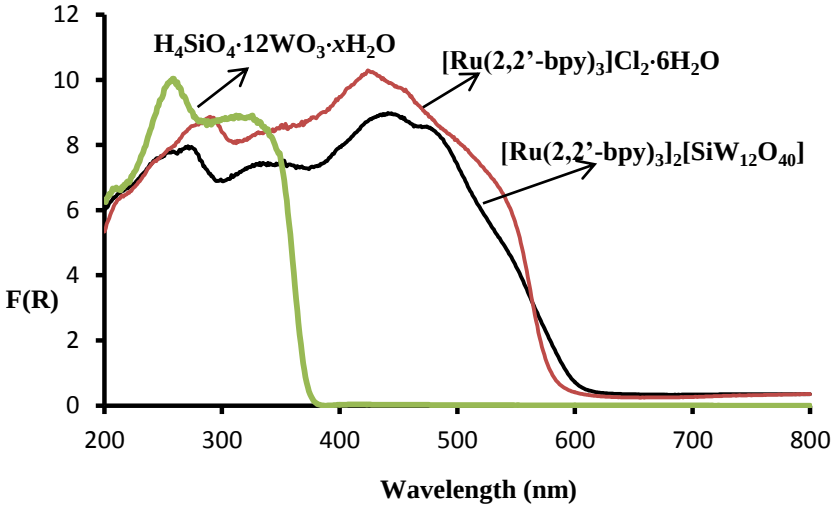

Figure 18. The UV/vis spectrum of compound **1** and $[Ru(2,2'\text{-bpy})_3]Cl_2\cdot 6H_2O$.

The UV-vis spectrum of compound **2** exhibits a broad band centered at 413 nm in visible range, which could be assigned to metal-to-ligand charge transfer (MLCT) band of $[Ru(2,2'\text{-bpy})_2(CH_3CN)_2]_2]^{2+}$. The bands at UV region are due to the (LMCT) transitions for W (VI) (O→W) and the π–π* transition of bpy ligand (Figure 3-7).

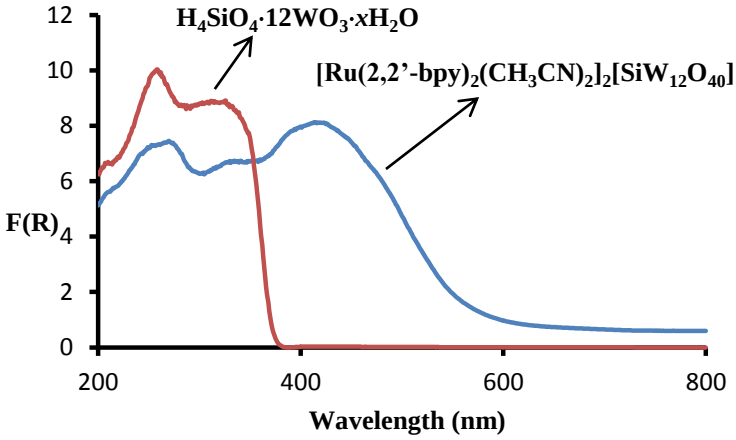

Figure 19. The UV/vis spectrum of compound **2**.

3.3.3 FT–IR Spectra

The FT-IR spectra are shown in figure 3-8 and the major vibration modes are listed in Table 3-5. Both hybrid complexes exhibit a band about 3078 cm^{-1}, which is the characteristic absorption of aromatic C−H stretch vibration of the 2,2'-bipyridine (2,2'-bpy) ligands. Both compounds display several absorption peaks located in the range of 1427−1635 cm^{-1}, which correspond to the characteristic vibrations of the 2,2'-bpy ligand of the photosensitizer cation.[77] Both compounds also show characteristic bands for $[SiW_{12}O_{40}]^{4-}$, namely, $\nu(W–O_t)$, $\nu(Si–O_a)$,$\nu(W–O_b)$ and $\nu(W–O_c)$ at 970, 921, 879, 794 cm^{-1}, for **1**, and at 970, 922, 882, 793 cm^{-1} for **2**.[78] In comparison with the Keggin-type complexes, $H_4SiO_4·12WO_3·xH_2O$, the peak shifts are observed (Figure 3-6 and Table 3-5). The higher energies for the W–O and Si–O stretches are consistent with a strong

interaction existing between POM anion with the dye $[Ru(2,2'\text{-}bpy_3)]^{2+}$ or $[Ru(2,2'\text{-}bpy)_2(CH_3CN)_2]_2]^{2+}$ cation in the hybrids.[79] For compound **1**, a strong band around 3526 cm^{-1} due to the presence of adsorpted moisture. The strong and broad peak around 3568 cm^{-1} in the IR spectrum of compound **2** can be attributed to the presence of adsorpted moisture. Bands at around 2980 and 2927 cm^{-1} are the characteristic absorption of saturated C−H stretch vibration of the CH_3CN ligands. The absorption bands at about 2350 and 2268 cm^{-1} usually come from C≡N triple bonds.[60]

Table 6. Major FT-IR peaks for $H_4SiO_4{\cdot}12WO_3{\cdot}xH_2O$, $[Ru(2,2'\text{-}bpy)_3]Cl_2{\cdot}6H_2O$, and the two hybrid compounds, **1** and **2** (cm^{-1}).

	Compound **1**	$H_4SiW_{12}O_{40}{\cdot}xH_2O$	$[Ru(2,2'\text{-}bpy)_3]Cl_2{\cdot}6H_2O$	Compound **2**
$\nu(Si\text{-}O_a)$	921	927		922
$\nu(W\text{-}O_t)$	970	980		970
$\nu(W\text{-}O_b)$	879	880		882
$\nu(W\text{-}O_c)$	794	784		793
2,2'-bpy	1429-1464		1421-1463	1427-1466
	1603-1635		1602-1654	1605-1624

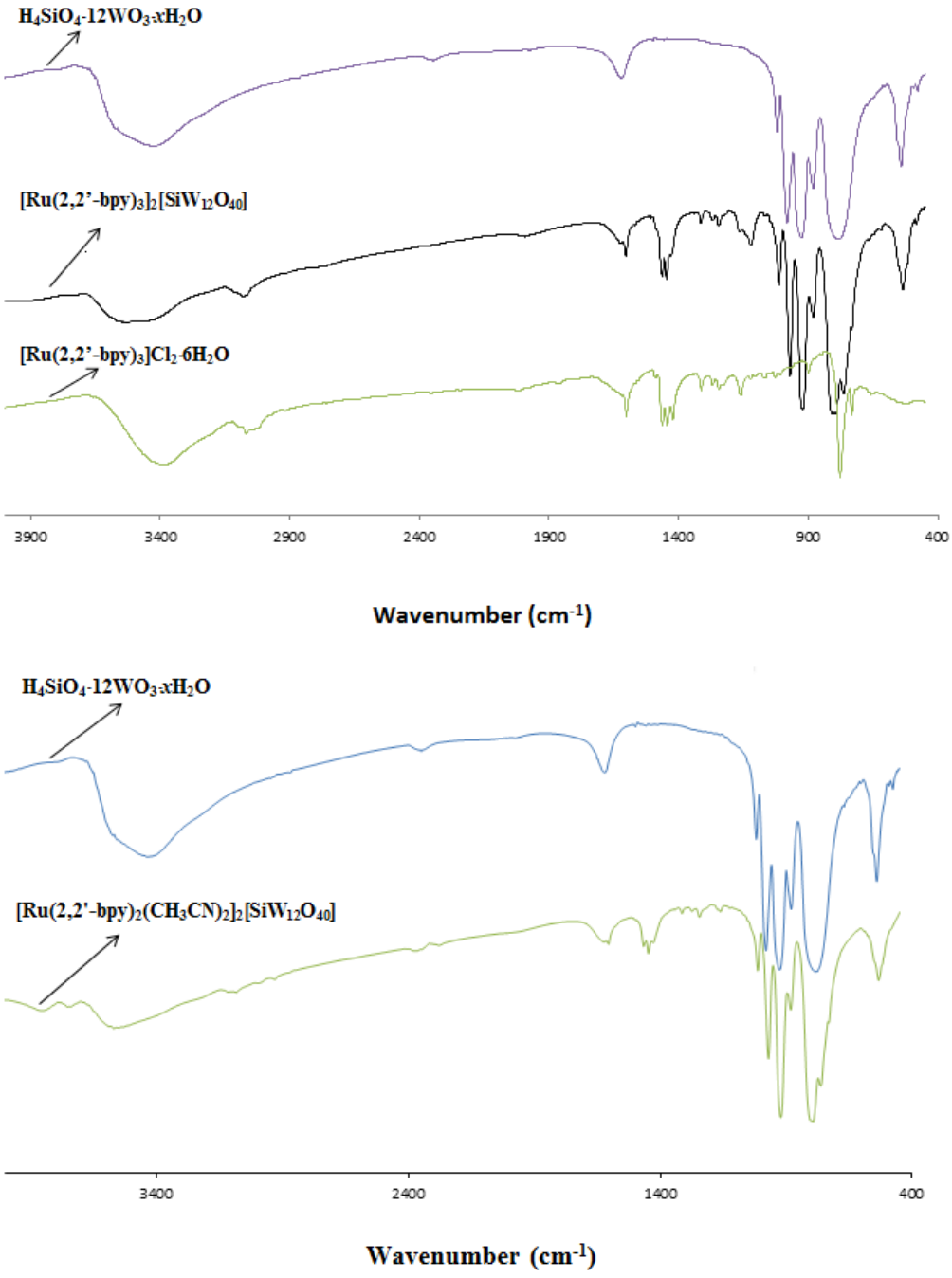

Figure 20. FT−IR spectrum of the ruthenium polypyridyl complex, tungstosilicic acid hydrate and the hybrid compounds.

3.3.4 TGA

The thermal stability of compounds **1** and **2** were investigated on powder samples in an air atmosphere in the temperature range 30-700^{o}C. The TG plot (Figure 3-9) of compound **1** shows a weight loss of 1.25% from 30 to 200^{o}C, which is attributed to the loss of adsorpted moisture. The weight loss of 23.24% in the temperature range 250-600^{o}C corresponds to the decomposition of 2,2'-bpy ligand molecules (calcd 23.14%). Compound **2** (Figure 3-10) shows a weight loss of 0.91% up to 182^{o}C, which is attributed to the loss of adsorpted moisture, followed by a weight loss of 20.26% at 183-600^{o}C, which corresponds to the decomposition of 2,2'-bpy and CH_3CN ligand molecules (calcd 20.22%).

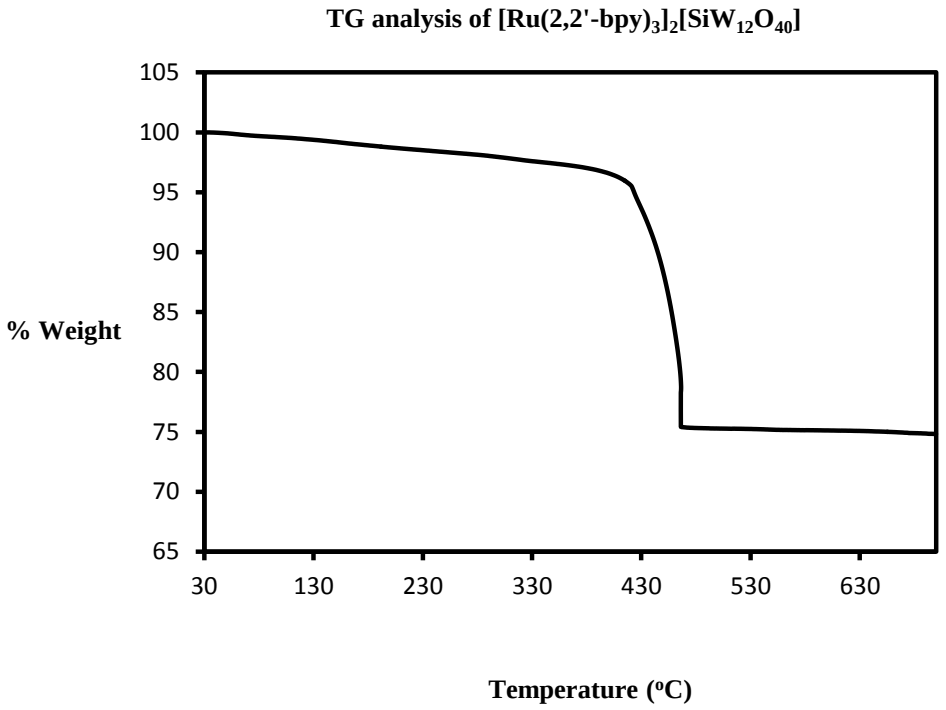

Figure 21. TG plot of $[Ru(2,2'\text{-bpy})_3]_2[SiW_{12}O_{40}]$

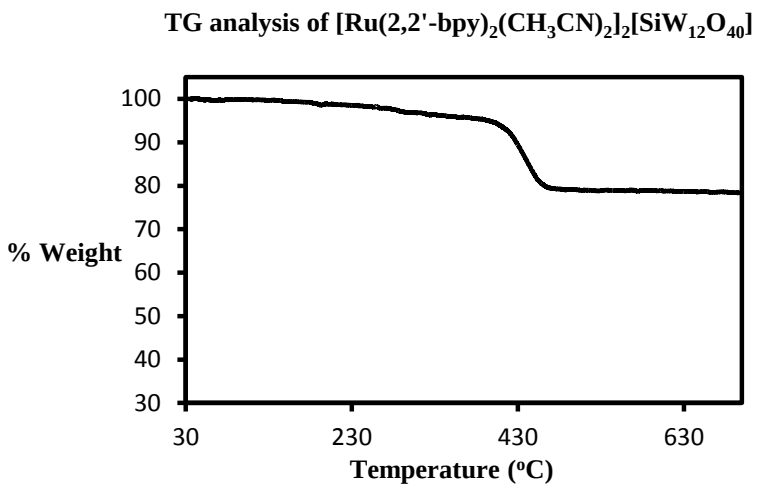

Figure 22. TG plot of $[Ru(2,2'\text{-}bpy)_2(CH_3CN)_2]_2[SiW_{12}O_{40}]$

3.3.5 Luminescence Spectrum

The luminescence spectrum of compound **1** as a suspension in water is shown in Figure 3-11. Upon excitation at the λ_{max} (450 nm) of the MLCT band of the $[Ru(bpy)_3]^{2+}$, an emission centered around 611 nm was observed, which can be attributed to the emission from the triplet MLCT excited state (^{3}MLCT) to the ground state.[80] This emission shows almost the same as $[Ru(2,2'\text{-}bpy)_3]Cl_2{\cdot}6H_2O$ in aqueous solution (around 610 nm at 293K)**.** No detectable luminescence has observed for compound **2**.

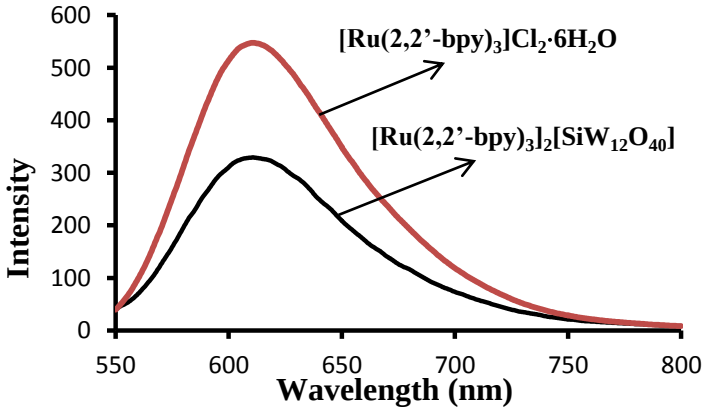

Figure 23. The luminescence spectrum of $[Ru(2,2'\text{-}bpy)_3]Cl_2{\cdot}6H_2O$ and $[Ru(2,2'\text{-}bpy)_3]_2[SiW_{12}O_{40}]$ excited at 450 nm.

3.4 Conclusions

Two organic-inorganic compounds, $[Ru(2,2'\text{-}bpy)_3]_2[SiW_{12}O_{40}]$ (**1**) and $[Ru(2,2'\text{-}bpy)_2(CH_3CN)_2]_2[SiW_{12}O_{40}]$ (**2**), have been synthesized and characterized. In both compounds **1** and **2**, the noncovalent interactions between Keggin ions and the Ru complexes connected the two units into three-dimensional networks. All the spectroscopic studies indicate that a strong interaction exists between the cationic dye and polyanion units. The $[Ru(2,2'\text{-}bpy)_3]^{2+}$ and its derivatives show great potential applications in the fields of artificial, photosynthesis, photovoltaics, photocatalysis and photoinduced water splitting due to interesting photochemical properties, and have been extensively investigated. In the future, we expect that modifying the ligands of $[Ru(2,2'\text{-}bpy)_3]^{2+}$ will allow the synthesis of solid materials containing Ru complexes linked to POM through coordination bonds and these materials with enhanced photochemical properties.

CHAPTER 4

Hybrid Solids Containing Tris-[2,2'-Bipyridine]Ruthenium(II) Chloride and Smaller POMs ($[W_6O_{19}]^{2-}$ or $[Mo_8O_{26}]^{4-}$)

ABSTRACT. Self-assembly of tris-[2,2'-bipyridine]ruthenium(II) chloride with smaller POMs ($[W_6O_{19}]^{2-}$ or $[Mo_8O_{26}]^{4-}$) produced two novel hybrid solids, $[Ru(2,2'\text{-}bpy)_3][W_6O_{19}]$ (**3**) and $[Ru(2,2'\text{-}bpy)_3]_2[Mo_8O_{26}]\cdot 5H_2O$ (**4**). These solids were characterized by elemental analysis, thermogravimetric analysis, spectroscopic methods as well as X-ray diffraction. X-ray crystallographic study showed that the crystal structures of both compounds were constructed by electrostatic attraction and C–H···O hydrogen bonds between tris-[2,2'-bipyridine]ruthenium(II) cations and polyanions ($[W_6O_{19}]^{2-}$ or $[Mo_8O_{26}]^{4-}$). Spectroscopic studies demonstrated that electronic communication occurred between smaller polyoxometalates and the sensitizer $[Ru(2,2'\text{-}bpy)_3]^{2+}$.

4.1 Introduction

In recent years, the synthesis of POM-dye hybrid materials has increased because of their potential application, but few studies on the details of the hybrid structure associated with the electron transfer process among these systems have been reported.[46] In this chapter, the synthesis and characterization of two hybrid POM-dye complexes,$[Ru(2,2'\text{-bpy})_3][W_6O_{19}]$ (**3**) and $[Ru(2,2'\text{-bpy})_3]_2[Mo_8O_{26}]\cdot 5H_2O$ (**4**) will be discussed. The structures of both compounds have been studied by X-ray diffraction. Spectroscopic studies demonstrated that electronic communication may occur between Lindqvist polyoxometalate and the sensitizer $[Ru(2,2'\text{-bpy})_3]^{2+}$.

4.2 Experimental

4.2.1 Synthesis

The reactions were carried out under hydrothermal conditions using 3"×4" Teflon bags in Teflon-lined stainless steel autoclave reactors.

Synthesis of compound **3**, (**$[Ru(2,2'\text{-bpy})_3][W_6O_{19}]$**). Cis-bis (2,2'-bipyridine) dichlororuthenium(II) hydrate (0.011 g), 2,2'-bipyridine (2,2'-bpy, 0.010 g) and deionized water (2 mL) were placed into a Teflon bag and then put in a 45 mL reaction vessel, and heated in an oven at 120^{o}C for 12 hours. After the autoclave was cooled to room temperature naturally, the red solution was transferred to another Teflon bag and added $3Na_2WO_4\cdot 9WO_3\cdot H_2O$ (0.110 g) and deionized water (2.0 mL). After that the Teflon bag was sealed and placed in a 45 mL reaction vessel and heated in an oven at 160^{o}C over 6 hours, held at that temperature for 96 hours, and then cooled down to room temperature over 6 hours. The red rectangular prism crystals of **3** were filtered, washed with deionized water, and dried in air (yield based on Ru: 63%). Elemental analysis:

calcd. for $C_{30}H_{24}RuN_6O_{19}W_6$: C, 18.23; H, 1.22; N, 4.25; *found*: C, 19.20; H, 1.16; N, 4.48%. FT-IR spectrum (KBr pellet, cm^{-1}): 3534 (broad), 3077 (s), 1602 (s), 1463(s), 1446(s), 975(s), 898(s), 807(s), 586(s). UV-visible (powder, λ_{max}/nm): 435.

Synthesis of compound **4**, **$[Ru(2,2'\text{-}bpy)_3]_2[Mo_8O_{26}]\cdot 5H_2O$**. 0.025 g of molybdic acid ($MoO_3\cdot H_2O$) and 2.0 mL of deionized water were placed into a Teflon bag, and then put in a warm water bath until molybdic acid was dissolved. 0.0124 g of tri-(2,2'-bipyridyl)dichloro-ruthenium(II) hexahydrate powder was dissolved in 2.0 mL of deionized water in another Teflon bag. The molybdic acid solution was then added into the tri-(2,2'-bipyridyl)dichloro-ruthenium(II) hexahydrate solution. After adding 2.0 M of potassium hydroxide, the mixture was changed from a turbid to a clear solution. 1.0 M of sulfate acid was used to adjust the pH to between 6.0 to 6.5. After that the Teflon bag was sealed and placed in a 45 mL reaction vessel and heated in an oven to 210^{o}C over 3 hours, held at that temperature for 72 hours, and then cooled down to room temperature over 3 hours. The red rhombohedral crystals of **4** were filtered, washed with deionized water, and dried in air (yield based on Ru: 62.6%). Elemental analysis: *calcd*. for $C_{60}H_{58}Mo_8N_{12}O_{31}Ru_2$: C, 29.86; H, 2.42; N, 6.97; *found*: C, 30.00; H, 2.10; N, 6.49%. FT-IR spectrum (KBr pellet, cm^{-1}): 3465 (broad), 3069 (s), 1602(s), 1463(s), 1446(s), 940(s), 913(s), 841(s). UV-visible (powder, λ_{max}/nm): 428.

4.2.2 X-ray Crystallography

X-ray diffraction data for compound **3** was collected on a Bruker Kappa Apex II CCD diffractometer with graphite monochromated Mo *K*α radiation (λ = 0.71073Å) at 293(2) K. Crystal data and relevant details of the structure determinations are summarized in Table 4-1 and selected geometrical parameters are given in Table 4-2.

Table 7. Crystallographic parameters and refinement details for compounds **3** and **4**.

	3	**4**
Formula	$C_{30}H_{24}N_6O_{19}RuW_6$	$C_{60}H_{58}N_{12}O_{31}Ru_2Mo_8$
Mol. wt.	1976.72	2412.84
Crystal system	Monoclinic	Monoclinic
Space group	$P2_1/n$ (14)	$P\ 2_1/c$ (14)
a (Å)	12.3326(4)	12.1940(1)
b(Å)	19.1085(6)	13.8280(1)
c(Å)	17.0984(5)	21.6890(2)
α(°)	90	90
β(°)	100.296(2)	91.3680(3)
γ(°)	90	90
V(Å^3)	3964.5(2)	3656.13(5)
Z	4	4
ρ (g/cm^3)	3.386	2.197
μ (mm^{-1})	17.794	1.820
Wavelength(Å)	0.71073	0.71073
Temperature(K)	296(2)	293(2)
Reflections collected/unique [R_{int}]	91965/8577[0.0769]	84230/8382[0.0449]
Goodness-of-fit(F^2)	1.194	1.122
Final R indices [$I > 2\sigma(I)$]	R_1= 0.0375,wR_2= 0.0665	R_1= 0.0338,wR_2= 0.0810
R indices (all data)	R_1= 0.0764,wR_2= 0.0850	R_1= 0.0421,wR_2= 0.0859

Table 8. Selected interatomic distances (Å) in compound **3** and **4**.

Complex 1		Complex 2	
W–O_t	1.695(3)-1.705(3)	Mo–O_t	1.700(3)-1.711(1)
W–$O_{\mu2}$	1.900(3)-1.937(7)	Mo–$O_{\mu2}$	1.754(1)-1.931(4)
W–$O_{\mu6}$	2.312(0)-2.332(0)	Mo–$O_{\mu3}$	1.949(5)-2.307(3)
		Mo–$O_{\mu5}$	2.143(0)-2.475(8)
Ru(1)–N(1)	2.055(6)	Ru(1)–N(38)	2.052(8)
Ru(1)–N(2)	2.053(0)	Ru(1)–N(36)	2.052(5)
Ru(1)–N(3)	2.056(5)	Ru(1)–N(37)	2.055(7)
Ru(1)–N(4)	2.065(2)	Ru(1)–N(41)	2.058(0)
Ru(1)–N(5)	2.074(8)	Ru(1)–N(39)	2.062(1)
Ru(1)–N(6)	2.070(8)	Ru(1)–N(40)	2.067(1)

4.3 Results and Discussions

Compounds **3** and **4** were synthesized using hydrothermal synthesis method. The tri-(2,2'-bipyridyl)dichloro-ruthenium(II) solution had to be made first by using cis-bis (2,2'-bipyridyl)dichloro-ruthenium(II) hydrate and excess 2,2'-bipyridine. Tri-(2,2'-bipyridyl)dichloro-ruthenium(II) hexahydrate couldn't be used directly because the quality of the crystals were insufficient for the single crystal X-ray diffraction study. Compound **3** can be crystallized in a neutral pH and in a temperature range of 160-190^{o}C. The resulting red rectangular prism crystals were obtained (Figure 4-1). In the synthesis of compound **4**, the molybdic acid solution had to be made first. The pH of the reaction mixture is critical for the crystallization of compound **4**. Potassium hydroxide had to be used to change the mixture from a turbid to a clear solution. The pH was adjusted to a range of 6.0 to 6.5 by adding sulfuric acid. Orange red rhombohedra crystals were formed (Figure 4-1). The products were not soluble in common solvents such as water, methanol, acetonitrile and DMF.

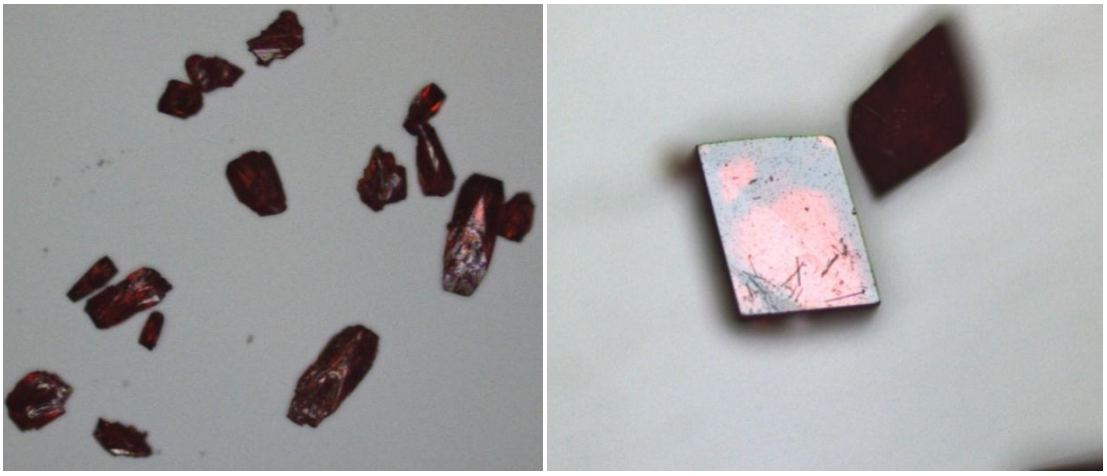

a b

Figure 24. (a) Stereomicroscope image of compound **3** (b) Stereomicroscope image of compound **4**.

4.3.1 Crystal Structure

Crystal structure of compound 3. Compound **3** crystallizes in the monoclinic space group $P2_1/n$. The structure of **3** consists of $[Ru(2,2'\text{-bpy})_3]^{2+}$ cationic complexes and Lindqvist ions $[W_6O_{19}]^{2-}$. Each $[W_6O_{19}]^{2-}$ presents as the ordered Lindqvist structure type with an approximate O_h symmetry.[81,82] The Lindqvist anion consists of six edge-sharing WO_6 octahedra with three types of W–O bond lengths: the W–$O_{\mu 6}$ lengths average in 2.320 Å for six-coordinated oxygen atoms, the W=O_t lengths average in 1.700 Å for the terminal oxygen atoms (O_t), and the remaining W–$O_{\mu 2}$ lengths average in 1.919 Å for the bridging oxygen atoms (Table 4-2).

There are extensive C–H···O hydrogen bonds between $[Ru(2,2'\text{-bpy})_3]^{2+}$ and $[W_6O_{19}]^{2-}$ in **3**. Some of the CH···O interactions are listed in Table 4-3. These interactions involve both terminal and bridged oxo groups of Linqvist ions. Each $[W_6O_{19}]^{2-}$ anion is hydrogen bonded to six $[Ru(2,2'\text{-bpy})_3]^{2+}$ cations, and in turn each $[Ru(2,2'\text{-bpy})_3]^{2+}$ cation hydrogen bonds to six $[W_6O_{19}]^{2-}$ anions to form a three-dimensional network (Figure 4-2). The hydrogen bonds between 2,2'-bpy and $[W_6O_{19}]^{2-}$ are relatively weak, with H···O contact in the range of 2.34-2.54 (1) Å. Because the sizes of these two ions are both close to 1 nm, the $[Ru(2,2'\text{-bpy})_3]^{2+}$ are evenly separated and have good contact with $[W_6O_{19}]^{2-}$ ions. The extensive hydrogen bonding between these two components provide path ways for possible electron transfer from $[Ru(2,2'\text{-bpy})_3]^{2+}$ to $[W_6O_{19}]^{2-}$ions under visible radiation.

Table 9. Atomic distance (Å) and angles (°) of $O_{POM}\cdots H_{pyr}$ interactions in the crystal structure of compound **3**.

Donor---H···Acceptor	d(D---H)	d(H····A)	d(D···A)	∠DHA
C(1)---H(1)···O(7)	0.93	2.52	3.39(5)	157
C(2)---H(2)···O(15)	0.93	2.47	3.27(1)	145
C(7)---H(7)···O(12)	0.93	2.54	3.15(6)	124
C(18)---H(18)···O(14)	0.93	2.53	3.24(0)	133
C(27)---H(27)···O(18)	0.93	2.47	3.14(1)	129
C(29)---H(29)···O(9)	0.93	2.34	3.12(3)	141

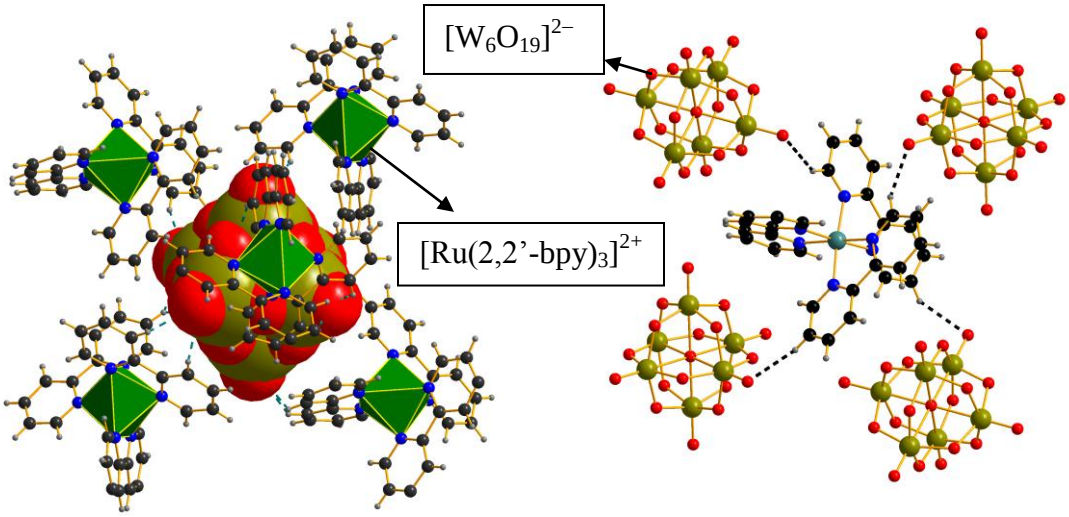

Figure 25. The $[Ru(2,2'\text{-bpy})_3]^{2+}$ cation linked to $[W_6O_{19}]^{2-}$ anions through hydrogen bonding.

Crystal structure of compound 4. There are five common isomers of $[Mo_8O_{26}]^{4-}$; α, β, γ, σ, and ε (Figure 4-3). The isomer structures of octamolybdates differ in number, types and fusion modes of molybdenum polyhedral. Unfortunately, the formation of a particular isomer in hydrothermal syntheses is not predictable.[83] The molybdate substructure of $[Ru(2,2'\text{-bpy})_3]_2[Mo_8O_{26}]\cdot 5H_2O$ is the σ-isomer of $[Mo_8O_{26}]^{4-}$ (Figure 4-4), which consists of two four-membered rings of eight MoO_6 octahedra. Four edge-sharing MoO_6 octahedra are co-planner to form a four-membered ring with common oxygen shared by the four edge-sharing MoO_6 octahedra.

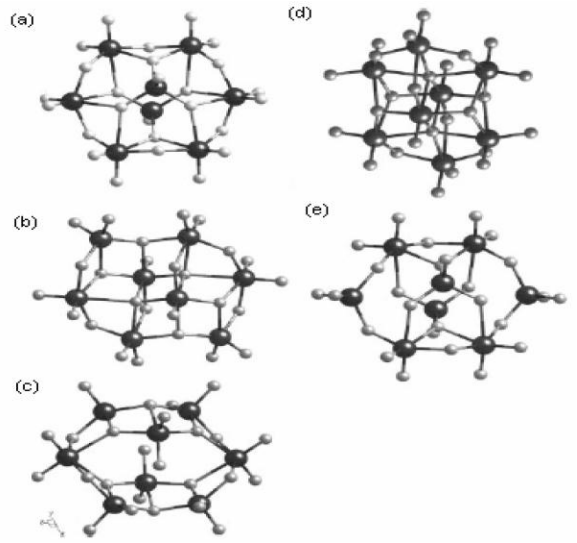

Figure 26. The structures of the a) α, b) β, c) γ, d) σ, and e) ε forms of $[Mo_8O_{26}]^{4-}$. [83]

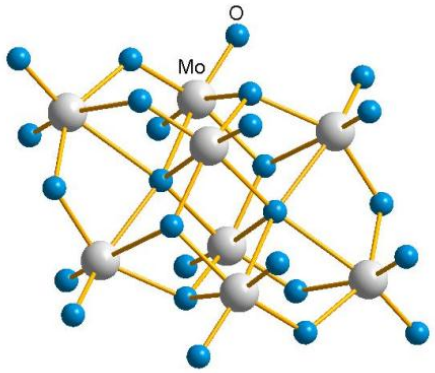

Figure 27. The σ-isomer of $[Mo_8O_{26}]^{4-}$ in compound **4**.

The crystal structure of compound **4** consists of σ–$[Mo_8O_{26}]^{4-}$, $[Ru(2,2'\text{-bpy})_3]^{2+}$ and lattice water molecules. There are also no "classical hydrogen bonds" between the $[Ru(2,2'\text{-bpy})_3]^{2+}$ cations and the σ–$[Mo_8O_{26}]^{4-}$ ion in **4** (Figure 4-5). Each $[Ru(2,2'\text{-bpy})_3]^{2+}$ unit forms hydrogen bonds with six $[Mo_8O_{26}]^{4-}$ cluster units through the C–H···O interactions in the range 2.37–2.54 Å (Table 4-4). These interactions play a significant role in the assembly of these ions into a solid. These non-covalent interactions not only help to hold the two types of fragments together, but also to direct the arrangement of these building units in the 3D space.

Table 10. Atomic distance (Å) and angles (°) of $O_{POM}\cdots H_{pyr}$ interactions in the crystal structure of compound **4**.

Donor---H···Acceptor	d(D---H)	d(H····A)	d(D···A)	∠DHA
C(22)---H(22)···O(9)	0.93	2.49	3.20(3)	134
C(25)---H(25)···O(6)	0.93	2.53	3.30(9)	142
C(33)---H(33)···O(12)	0.93	2.54	3.41(8)	157
C(45)---H(45)···O(7)	0.93	2.38	3.23(7)	153
C(49)---H(49)···O(10)	0.93	2.52	3.42(6)	166
C(50)---H(50)···O(11)	0.93	2.50	3.21(3)	134
C(55)---H(55)···O(14)	0.93	2.46	3.18(9)	135
C(57)---H(57)···O(18)	0.93	2.37	2.24(8)	158

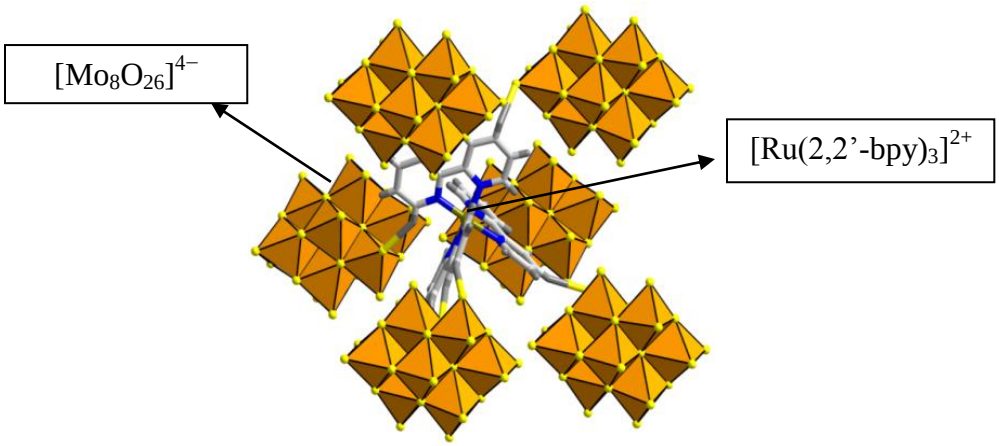

Figure 28. The $[Ru(2,2'\text{-bpy})_3]^{2+}$ cation linked to $[Mo_8O_{26}]^{4-}$ anions through hydrogen bonding.

The phase purity of compounds **3** and **4** were confirmed by comparing the powder X-ray diffraction (PXRD) patterns of the pristine sample and the simulated pattern from the crystal structure. Compound **4** was a pure product based on the agreement of their PXRD diffraction patterns and the simulate patterns (Figure 4-6).

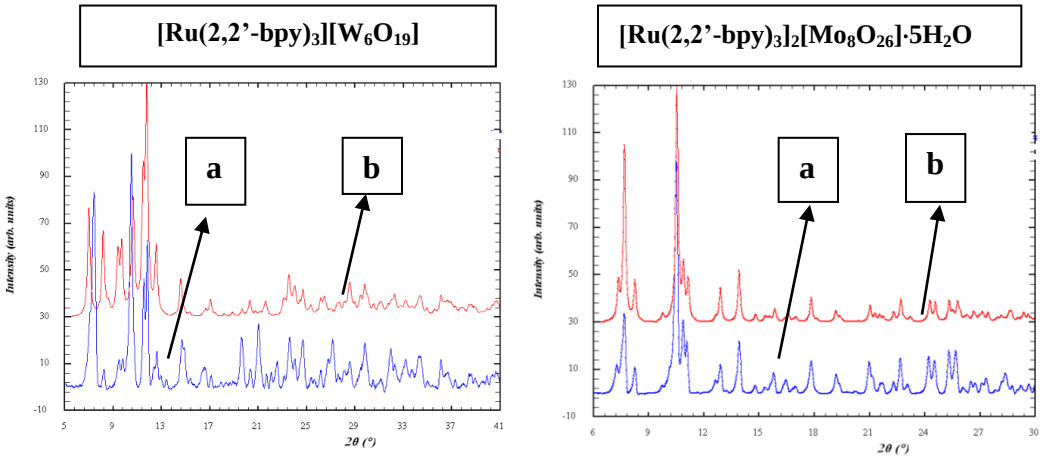

Figure 29. The powder X-ray diffraction patterns (blue line, a) and the simulated patterns (red line, b) of compound **3** and **4**.

4.3.2 UV-vis Diffuse Reflectance Spectra

Fig. 4-7 displays the UV-vis diffuse reflectance spectra of [Ru(2,2'-bpy)$_3$]Cl$_2$·6H$_2$O, compounds **3** and **4**. Both compounds **3** and **4** show the characteristic band of [Ru(2,2'-bpy)$_3$]$^{2+}$, at 435, and at 427 nm for **3**, and **4** respectively. These bands can be attributed to the metal-to-ligand charge transfer (MLCT) transition in which electrons located in metal-based d orbitals are promoted into ligand-centered π* orbitals.[12b] The λ_{max}(435, 427 nm) of MLCT bands of compounds **3** and **4** shows a red shift in comparison with [Ru(2,2'-bpy)$_3$]Cl$_2$·6H$_2$O (λ_{max}= 422 nm). The UV absorption band at ~274 nm corresponds to a ligand-centered π–π* transition of 2,2'-bpy ligand.[76] The λ_{max} of UV absorption bands of compounds **3** and **4** shows a blue shift in comparison with [Ru(2,2'-bpy)$_3$]Cl$_2$·6H$_2$O (λ_{max}= 290 nm). These new charge transfer transitions in compounds **3** and **4** indicate electronic communication occurred between the polyoxometalates and the sensitizers.

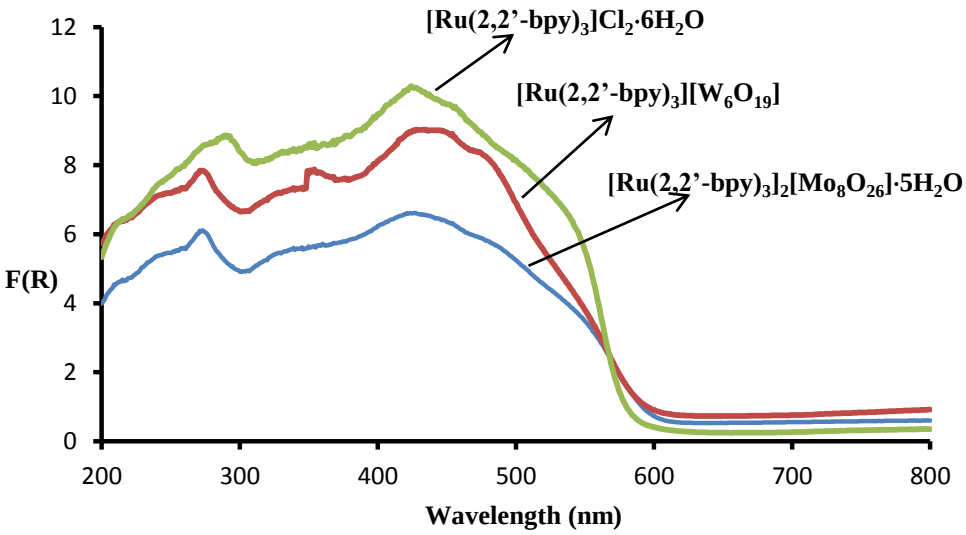

Figure 30. The UV/vis spectrum of compounds **3**, **4** and $[Ru(2,2'\text{-bpy})_3]Cl_2 \cdot 6H_2O$.

4.3.3 FT-IR Spectra

The FT-IR spectra of compound **3** (Figure 4-8) show a strong band around 3534 cm^{-1} due to the presence of water molecules. The strong bands at 975, 898, 807 and 586 cm^{-1}(W–O) are typical of $[W_6O_{19}]^{2-}$.[84,85] The peaks in the range 1435-1614 cm^{-1} are characteristic of 2,2'-bpy.[78] The strong and broad peak around 3456 cm^{-1} in the IR spectrum of compound **4** (Figure 4-8) can be attributed to the presence of water molecules. The strong bands at 940 and 913 cm^{-1} are attributed to the Mo=O stretching, while multiple bands attributed to the bridging (Mo–O–Mo) groups' absorptions are found in the 450–841 cm^{-1} region.[86] The peak in about 3069 cm^{-1} is the characteristic absorption of aromatic C–H stretch vibration of the 2,2'-bipyridine ligands.[60]

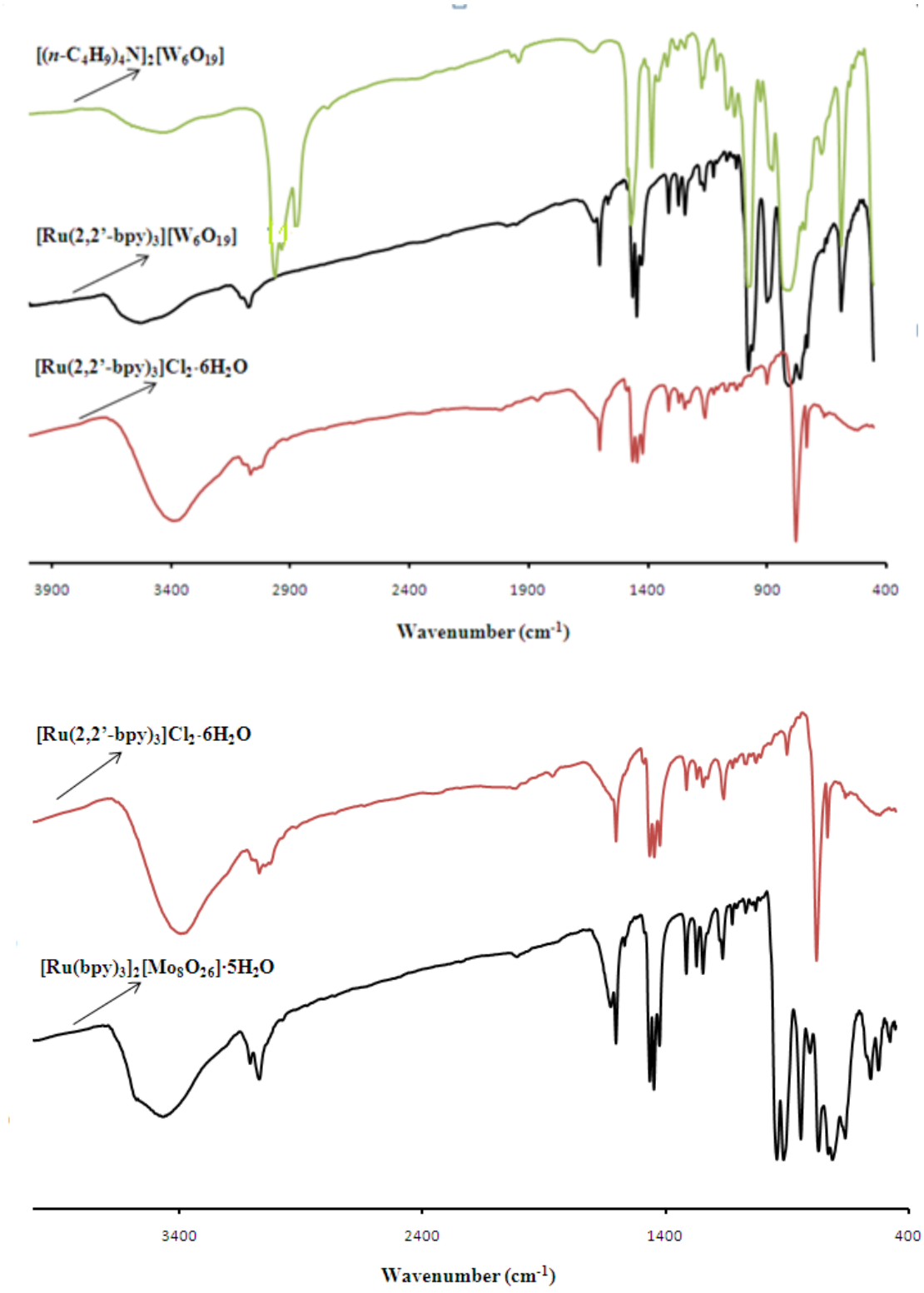

Figure 31. FT-IR spectrum of $[Ru(2,2'\text{-}bpy)_3]^{2+}$, smaller POMs and hybrid compounds.

4.3.4 TGA

The thermal behavior of compounds **3** and **4** were investigated on powder samples in an air atmosphere in temperature range 40-700^{o}C. The TG curve (Figure 4-9) of compound **3** exhibited two steps of weight loss. The first weight loss was 1.32% in the temperature range from 40 to 200^{o}C, which is attributed to the loss adsorpted moisture. The weight loss of 24.53% from 250 to 600^{o}C is corresponding to the decomposition of 2,2'-bpy ligand molecules (calcd 23.49%). Compound **4** (Figure 4-10) shows a weight loss of 3.4% from 40 to 200^{o}C, which is attributed to the loss of water molecules (calcd 3.73%), followed by a weight loss of 37.9% at 250 -700^{o}C, which is corresponding to the decomposition of 2,2'-bpy ligand molecules (calcd 38.8%).

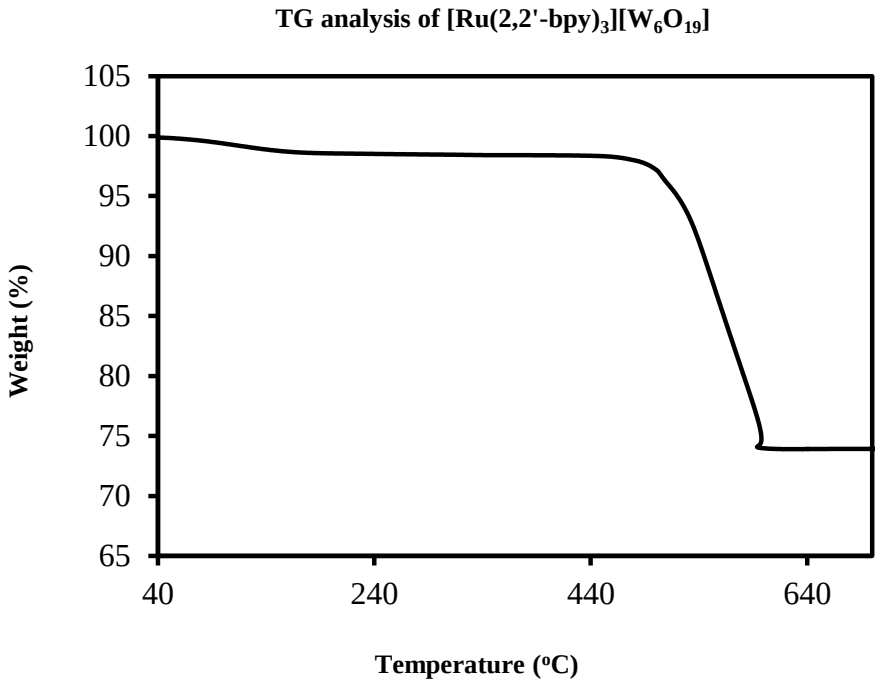

Figure 32. TG plot of TG analysis of [Ru(2,2'-bpy)$_3$][W_6O_{19}].

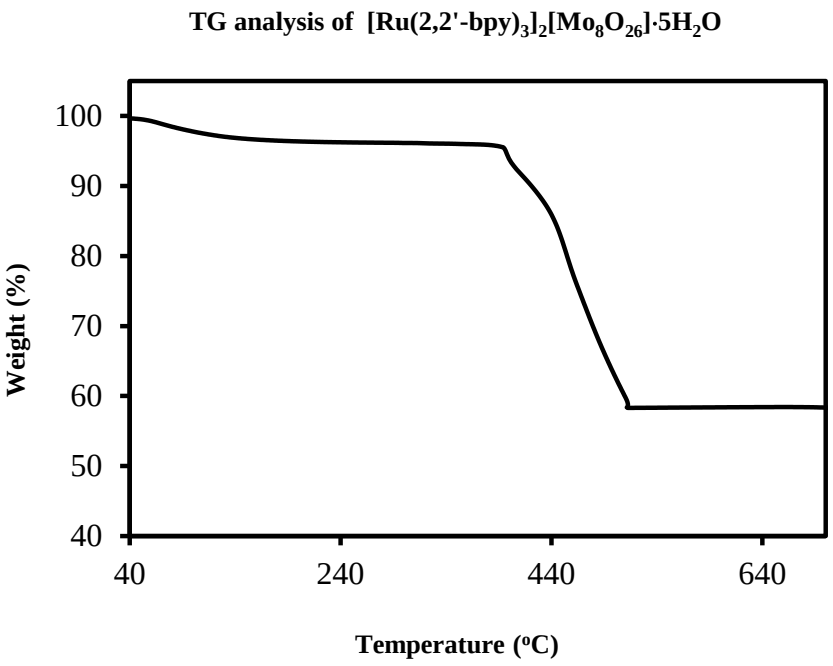

Figure 33. TG plot of $[Ru(2,2'\text{-}bpy)_3]_2[Mo_8O_{26}]\cdot 5H_2O$.

4.3.5 Luminescence Spectrum

The luminescence spectra of compounds **3** and **4** as a suspension in water are shown in Figure 4-11. Upon excitation at the λ_{max} (450 nm) of the MLCT band of the $[Ru(2,2'\text{-}bpy)_3]^{2+}$, compound **3** shows an emission centered at 599 nm and compound **4** displays an emission centered at 613 nm, which can be attributed to the emission from the triplet MLCT excited state (^{3}MLCT) to the ground state.[80] The emission of compound **3** exhibits a blue-shift in comparison with that of $[Ru(2,2'\text{-}bpy)_3]^{2+}$ in aqueous solution (610 nm). The emission spectrum of compound **4** shows a slight red-shift in comparison with that of $[Ru(2,2'\text{-}bpy)_3]^{2+}$ in aqueous solution (610 nm). All these changes mentioned above may be associated with the strong interactions between tris-(2,2'-bipyridine)ruthenium(II) and the polyanion, which have influence on the molecular orbitals of ligands and metal ion in $[Ru(2,2'\text{-}bpy)_3]^{2+}$.

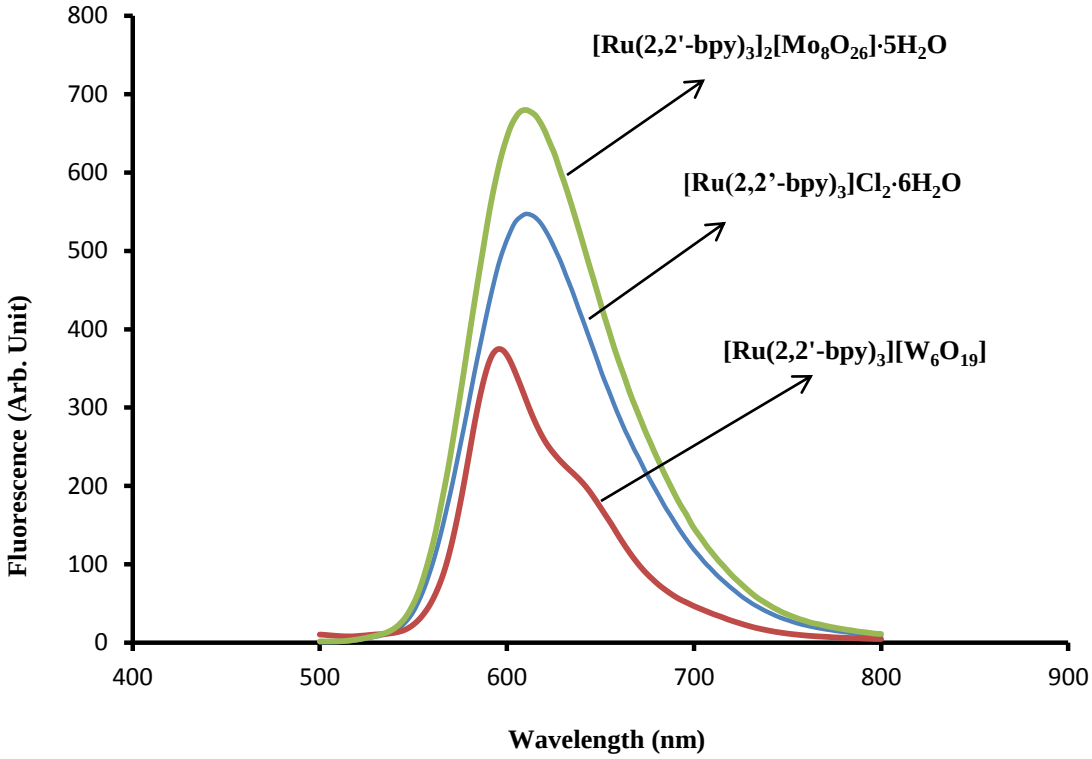

Figure 34. The luminescence spectrum of compounds **3**, **4** and $[Ru(2,2'\text{-}bpy)_3]Cl_2{\cdot}6H_2O$ excited at 450 nm.

To explore the impact of $[W_6O_{19}]^{2-}$ on the photophysics of $[Ru(2,2'\text{-}bpy)_3]^{2+}$, steady state quenching studies were conducted (Figure 4-12) in dry acetonitrile. As observed for the interaction of $[W_6O_{19}]^{2-}$ with $[Ru(2,2'\text{-}bpy)_3]^{2+}$, addition of increasing concentrations of $[W_6O_{19}]^{2-}$ resulted in significant quenching of the $[Ru(2,2'\text{-}bpy)_3]^{2+}$ excited state. The luminescence intensity of $[Ru(2,2'\text{-}bpy)_3]^{2+}$ (2×10^{-4}M) decreased progressively with increasing concentrations of $[W_6O_{19}]^{2-}$.

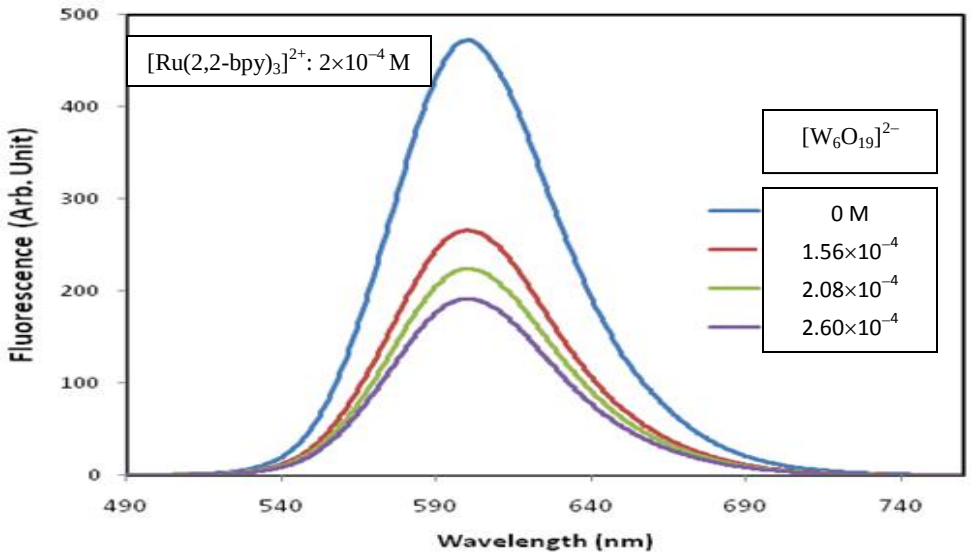

Figure 35. Luminescence spectrum in dry acetonitrile of $[Ru(2,2'\text{-bpy})_3]^{2+}$ (2×10^{-4} M) on addition of incremental amounts of $[W_6O_{19}]^{2-}$.

4.4 Conclusions

Two novel hybrid compounds containing smaller POM clusters and ruthenium(II) polypyridine complexes have been hydrothermally synthesized and structurally characterized. The successful isolation of compounds **3** and **4** demonstrates that the hydrothermal method can be used for the incorporation of photosensitizers such as $[Ru(2,2'\text{-bpy})_3]^{2+}$ into solid compounds to form hybrid materials. The non-covalent interactions play an important role in the assembly of the building blocks into solids. They direct the arrangement of these building units in the 3D space and the formation of 3D structures. This provides an alternative method for the synthesis of multi-component photoactive systems for energy transfer or charge separation to conventional methods using covalent bond interactions. Spectroscopic studies demonstrated that electronic communication between the ions was detected in compounds **3** and **4**, including observation of new optical transitions in the spectroscopic studies.

CHAPTER 5

Conclusion

The synthesis and characterization of organic-inorganic solid state hybrid materials has attracted great attention due to their chemistry and widely promising potential applications in sensors, selective membranes, electrochemical devices, supported catalysts or photo electrochemical energy conversion cells.[1]

In this thesis, the synthesis, structures and properties of hybrid solid materials containing ruthenium polypyridyl complexes and polyoxometalate anions have been described. Our experimental results showed that the self-assembly of polyoxometalates and ruthenium polypyridyl complexes into hybrid solids can be carried out by the hydrothermal method or through the room temperature solution approach.

Four new compounds have been synthesized. Compound **1**, $[Ru(2,2'\text{-}bpy)_3]_2[SiW_{12}O_{40}]$, crystallizes in the triclinic space group $P\bar{1}$. It consists of Keggin anion $[SiW_{12}O_{40}]^{4-}$and charge balancing cation $[Ru(2,2'\text{-}bpy)_3]^{2+}$. Each $[SiW_{12}O_{40}]^{4-}$anion is hydrogen bonded to eight $[Ru(2,2'\text{-}bpy)_3]^{2+}$ cations, and in turn each $[Ru(2,2'\text{-}bpy)_3]^{2+}$cation is hydrogen bonded to four $[SiW_{12}O_{40}]^{4-}$ anions. CH···O interactions involve both terminal and bridged oxo groups of Keggin ions. Compound **2**, $[Ru(2,2'\text{-}bpy)_2(CH_3CN)_2]_2[SiW_{12}O_{40}]\cdot 2H_2O$, has the same Keggin cluster ion $[SiW_{12}O_{40}]^{4-}$ as compound **1**. An interesting feature of compound **2** is that the Ru(II) ion coordinates to two 2,2'-bipyridine ligands and two acetonitrile ligands. Bond length for Ru-N is in the range of 2.013(1)-2.060(1) Å. The Ru-N bond lengths are shorter than those in compound **1**. Compound **3**, $[Ru(2,2'\text{-}bpy)_3][W_6O_{19}]\cdot 1.5H_2O$, crystallizes in the monoclinic space group $P2_1/n$. The structure of **3** consists of $[Ru(2,2'\text{-}bpy)_3]^{2+}$ cationic complexes and

Lindqvist ions $[W_6O_{19}]^{2-}$. Each $[W_6O_{19}]^{2-}$ presents as the ordered Lindqvist structure type with an approximate O_h symmetry. Compound **4**, $[Ru(2,2'\text{-bpy})_3]_2[Mo_8O_{26}]\cdot 5H_2O$, consists of σ–$[Mo_8O_{26}]^{4-}$, $[Ru(2,2'\text{-bpy})_3]^{2+}$ and lattice water molecules. The σ-isomer of $[Mo_8O_{26}]^{4-}$ consists of two four-membered rings of eight MoO_6 octahedra. Four edge-sharing MoO_6 octahedra are co-planner to form a four-membered ring with common oxygen shared by the four edge-sharing MoO_6 octahedra.

Compounds **1**, **3**, and **4** were synthesized using hydrothermal synthesis method. Compound **2** was synthesized in one-step reaction by simply mixing solutions of the reactants. As expected, control of the pH of the reaction mixtures is critical for the crystallization of these compounds. For example, compound **1** only can be crystallized in narrow pH at around 2; Compound **3** can be crystallized in a neutral pH; Compound 4 can be crystallized in a near neutral pH which is adjusted by potassium hydroxide and sulfate acid. These new hybrid solid materials are insoluble in common solvents such as water, methanol, acetonitrile and DMF.

X-ray crystallographic study showed that Coulombic forces and supramolecular interactions play an important role in the assembly of the crystal structures of compounds **1**, **2**, **3** and **4**. These hybrid compounds were connected and formed 3D structure through $C–H\cdots O_{POM}$ and other weak interactions. These noncovalent interactions between POMs and ruthenium polypyridyl complexes provided an alternative method for the synthesis of multi-component photoactive systems for energy transfer or charge separation to conventional methods using covalent bond interactions.

In the UV-vis diffuse reflectance spectra, all new hybrid solid materials exhibit the characteristic band of $[Ru(2,2'\text{-bpy})_3]^{2+}$. These bands can be attributed to the metal-

to-ligand charge transfer (MLCT) transition in which electrons located in metal-based d orbitals are promoted into ligand-centered π* orbitals. The λ_{max} (445, 435, 427 nm) of MLCT bands of compounds **1**, **3** and **4** shows a red shift in comparison with [Ru(2,2'-bpy)$_3$]Cl$_2$·6H$_2$O (λ_{max}= 422 nm). Compound **1**, **3** and **4** have luminescence. Upon excitation at the λ_{max} (450 nm) of the MLCT band of the $[Ru(bpy)_3]^{2+}$, compound **1** exhibits an emission centered around 611 nm; compound **3** shows an emission centered at 599 nm; and compound **4** displays an emission centered at 613 nm, which can be attributed to the emission from the triplet MLCT excited state (^{3}MLCT) to the ground state. The emission of compound **3** exhibits a blue-shift in comparison with that of $[Ru(2,2'\text{-}bpy)_3]^{2+}$ in aqueous solution (610 nm). The steady state quenching study of compound **3** shows that addition of increasing concentrations of $[W_6O_{19}]^{2-}$ results in significant quenching of the $[Ru(2,2'\text{-}bpy)_3]^{2+}$ excited state. These spectroscopic studies demonstrated that strong electronic communication occurred between the cationic dye and polyanion units. Thermogravimetric analysis (TGA) shows that the 2,2'-bipyridine ligands of new hybrid materials start decomposition around 200^{o}C. It means there are stable under routine temperature. Studies are underway to investigate the photocatalytic properties of these novel solids.

In the future we expect that modifying the ligand of $[Ru(2,2'\text{-}bpy)_3]^{2+}$ will allow the synthesis of solid materials containing Ru complexes linked to POM through coordination bonds and these materials with enhanced photochemical properties.

REFERENCES

1. Chujo, Y. *KONA*. **2007**, *25*, 255-259.
2. Judeinstein, P.; Sanchez, C. *J. Mater. Chem*. **1996**, *6*, 511-525.
3. Bi, L. H.; Hou, G. F.; Bao, Y. Y.; Li, B.; Wu, L. X.; Gao, Z. M.; McCormac, T.; Mal, S. S.; Dickman, M. H.; Kortz, U. *Eur. J. Inorg. Chem*. **2009**, 5259-5266.
4. Balzani, V. *Pure & Appl. Chem.***1990**, *62* (6), 1099-1102.
5. (a) Sun, L.; Akermark, B.; Ott, S. *Coordination Chemistry Reviews*. **2005**, *249*, 1653-1663.

   (b) Richter, M. M. *Chem. Rev*. **2004**, *104*(6), 3003-3006.
6. Gomez-Romero, P. *Adv. Mater*. **2001**, *13*, 163-174.
7. Kickelbick, G. *Hybrid Materials*. Wiley-VCH Verlag: Wemheim, **2006**.
8. Gomez-Romero, P.; Sanchez, C. *Functional Hybrid Materials*. Wiley-VCH Verlag: Wemheim, **2003**.
9. Dolbecq, A.; Dumas, E.; Mayer, C. R.; Mialane, P. *Chem. Rev*. **2010**, *110*, 6009-6048.
10. Campagna, S.; Puntoriero, F.; Nastasi, F.; Bergamini, G.; Balzani V. *Chemistry and Materials Science.* **2007**, *280*, 117-214.
11. (a) Van Houten, J.; Watts. R. J. *Inorg. Chem*. **1978**, *17*(12), 3381-3385.

    (b) Seery, M. K.; Guerin, L.; Forster, R. J.; Gicquel, E.; Hultgren, V.; Bond, A. M.; Wedd, A. G.; Keyes, *T. E. J. Phys. Chem. A*. **2004**, *108*, 7399-7405.

    (c) Falkenstrom, M.; Johansson, O.; Hammarstrom, L. *Inorganica Chimica Acta*. **2007**, *360*, 741-750.
12. (a) Meyer, T. J. *Pure & Appl. Chem*. **1986**, *58*(9), 1193-1206.

(b) Damrauer, N. H.; Cerullo, G.; Yeh, A.; Boussie, T. R.; Shank, C. V.; McCusher, J. K. *Science.* **1997**, *275*, 54-57.

(c) Mori, K.; Kawashima, M.; Che, M.; Yanmashita, H. *Angew. Chem. Int. Ed.* **2010**, *49*, 1-5.

(d) Caspar, J. V.; Meyer, T. J. *Inorg. Chem*. **1983**, *22*(17), 2444-2453.

(e) Kober, E. M.; Patrick Sullivan, B.; Meyer, T. J. *Inorg. Chem*. **1984**, *23*(14), 2098-2104.

13. Juris, A.; Campagna, S.; Balzani, V.; Gremaud, G.; Zelewsky, A. V. *Inorg. Chem*. **1988**, *27*(20), 3652-3655.
14. (a) Desilvestro, J.; Graetzel, M.; Kavan, L.; Moser, J.; Augustynski, J. *J. Am. Chem. Soc*. **1985**, *107*(10), 2988-2990.

    (b) Vlachopoulos, N.; Liska, P.; Augustynski, J.; Graetzel, M. *J. Am. Chem. Soc*. **1988**, *110*(4), 1216-1220.

    (c) Amadelli, R.; Argazzi, R.; Bignozzi, C. A.; Scandola, F. *J. Am. Chem. Soc*. **1990**, *112*(20), 7099-7103.

    (d) Nazeeruddin, Md. K.; Zakkeeruddin, S. M.; Humphry-Baker, R.; Jirousek, M.; Liska, P.; Vlachopoulos, N.; Shklover, V.; Fischer, Christian-H.; Gratzel. M. *Inorg. Chem*. **1999**, *38*, 6298-6305.
15. Brown, G. M.; Callahan, R. W.; Meyer, T. J. *Inorg. Chem*. **1975**, *14*(8), 1915-1921.
16. Singh, T. N.; Turro, C. *Inorg. Chem*. **2004**, *43*(23), 7260-7262.
17. (a) Durham, B.; Walsh, J. L.; Carter, C. L.; Meyer, T. J. *Inorg. Chem*. **1980**, *19*, 860-865.

(b) Wu, Q.; Wang, L. *Synthesis*. **2008**, *13*, 2007-2012.

18. Wight, A. P.; Davis, M. E. *Chem. Rev*. **2002**, *102*, 3589-3614.
19. Browne, W. R. *Coordination Chemistry Reviews*. **2008**, *252*, 2470-2479.
20. (a) Pope, M. T.; Muller, A. *Angew. Chem., Int. Ed. Engl*. **1991**, *30*, 34.

    (b) Pope, M. T.; Muller, A.; Eds. *Polyoxometalates: from Platonic Solids to Anti-retroviral Activity*. Kluwer: Dordrecht, **1994**.
21. Pope, M. T. *Heteropoly and Isopoly Oxometalates*. Springer: New York, **1983**.
22. Borras-Almenar, J. J.; Coronado, E.; Muller, A.; Pope, M. *Polyoxometalate Molecular Science*. Kluwer: Dordrecht, **2001**.
23. Kozhevnikov, I. V. *Catalysis by Polyoxometalates.* Wiley: Chichester, **2002**.
24. Contant, R. *Inorg. Synth*. **1990**, *27*, 80-105.
25. (a) Hiskia, A.; Mylonas, A.; Papaconstantinou, E. *Chem. Soc. Rev.* **2001**, *30*, 62-69.

    (b) Long, D. L.; Tsunashima, R.; Cronin, L. *Angew. Chem. Int. Ed.* **2010**, *49*, 1736-1758.
26. Berzelius, J. J. *Pogg. Ann*. **1826**, *61*, 380.
27. Svangerg, K.; Struve, H. *J. Prakt. Chem.* **1848**, *44*, 257-291.
28. Keggin, J. F. *Nature*, **1933**, *131*, 908-909.
29. (a) Clemente-Leon, M.; Agricole, B.; Mingotaud, C.; Gomez-Garciz, C.J.; Coronado. E.; Delhaes. P. *Langmuir*. **1997**, *13*, 2340-2347.

    (b) Maestre, J. M.; Lopez, X.; Bo, C.; Poblet, J.; Casan-Pastor, N. *J. Am. Chem. Soc*. **2001**, *123*, 3749-3758.
30. (a) Akid, R.; Darwent, J. R. *J. Chem. Soc. Dalton Trans.* **1985**, 395-399

(b) Li, Y.; Ren, C.; Peng, S.; Lu, G.; Li, S. *Journal of Molecular Catalysis A: Chemical*. **2006**, 246, 212-217

31. Carey, D. M.; Munoz-Castro, A.; Bustos, C. J.; Manriquez, J. M; Arratia-Perez, R. J. *Phys. Chem. A*. **2007**, *111*, 6563-6567.
32. (a) Sharpless, K. B.; Patrick, D. W.; Truesdale, L. K.; Biller, S. A. *J. Am. Chem. Soc*. **1975**, *97*, 2305-2307.

    (b) Chong, A. O.; Oshima, K.; Sharpless, K. B. *J. Am. Chem. Soc*. **1977**, *99*, 3420-3426.
33. (a) Graselli, R. K.; Burrington, J. D. *Ind. Eng. Chem. Prod. Res. Develop*. **1984**, *23*, 393-404.

    (b) Burrington, J. D.; Kartisek. C. T.; Graselli, R. K. *J. Catal*. **1983**, *81*, 489-498.
34. Yang, X.; Waters, T.; Wang, X. B.; O'Hair, R. A.; Wedd, A. G.; Li, J.; Dixon, D. A.; Wang, L. S. *J. Phy. Chem. A*.**2004**, *108*, 10089-10093.
35. Bannani, F.; Driss, H.; Thouvenot, R.; Debbabi, M. *Journal of Chemical Crystallography*. **2007**, *37*(1), 37-48.
36. Che, T. M.; Day, V. W.; Francesconi, L. C.; Fredrich, M. F.; Klemperer, W. G.; Shum, W. *Inorg. Chem.***1985**, *24*(24) 4055-4062.
37. Troupis, A.; Hiskia, A.; Papaconstantinou, E. *Angew. Chem. Int. Ed.* **2002**, *41*, 1911-1914.
38. Yamase, T. *Chem. Rev*. **1998**, *98*, 307-325.
39. Fay, N.; Dempsey, E.; Kennedy, A.; McCormac, T. *J. Electroanal. Chem.* **2003**, *556*, 63.

40. Fay, N.; Hultgren, V. M.; Wedd, A. G.; Keyes, T. E.; Forster, R. J.; Leane, D.; Bond, A. M. *Dalton Trans*. **2006**, *35*, 4218.

41. Seery, M. K.; Fay, N.; McCormac, T.; Dempsey, E.; Forster, R. J.; Keyes, T. E. *Phys. Chem. Chem. Phys.***2005**, *7*, 3426-3433.

42. (a) Wang, X. L.; Han, Z. B.; Wang, E. B.; Zhang, H.; Hu, C. W. *Electroanalysis*, **2003**, *15*, 1460.

    (b) Wang, X. L.; Zhang, Q.; Han, Z. b.; Wang, E. B.; Guo, Y. Q.; Hu, C.W. *J. Electroanal. Chem.***2004**, *563*, 221.

43. Bi, L. H.; Zhou, W. H.; Wang, H. Y.; Dong, S. J. *Electroanalysis*. **2008**, *20*(9), 996-1001.

44. Han, Z. B.; Wang, E. B.; Luan, G. Y.; Li, Y. G.; Hu, C. W.; Wang, P.; Hu, N. H.; Jia, H. Q. *Inorg. Chem. Commun*. **2001**, *4*, 427.

45. Yan, B.; Hodsdon, S. A.; Li, Y. F.; Carmichael, C. N.; Cao, Y.; Pan, W. P. *Journal of Solid State Chemistry*. **2011**, *184*(12), 3179-3184.

46. Song, J.; Luo, Z.; Zhu, H.; Huang, Z.; Lian, T.; Kaledin, A.; Musaev, D. G.; Lense, S.; Hardcastle, K. I.; Hill, C. L. *Inorganica Chimica Acta*. **2010**, *363*(15), 4381-4386.

47. Han, Z.; Wang, E.; Luan, G.; Li, Y.; Hu, C.; Wang, P.; Hu, N.; Jia, H. *Inorganic Chemistry Communications*. **2001**, *4*, 427-429.

48. Byrappa, K.; Yoshimura, M. *Handbook of Hydrothermal Technology*. Noyes Publications/William Andrew Publishing LLC: New York, **2001**.

49. Rabenau, A. *Angew. Chem., Int. Eng. Ed*. **1985**, *24*, 1026-1040.

50. Morey, G. W.; Niggli, P. *J. Am. Chem. Soc*. **1913**, *35*, 1086-1130.

51. Roy, R. *J. Solid State Chem*. **1994**, *111*, 11-17.

52. Van der Put, P. J. *The Inorganic Chemistry of Materials-How to Make Things out of Elements.* Plenum Press: New York and London, **1998**, 273-316.

53. Hojamberdiev, M.; Xu, Y.; Wang, F.; Wang, J.; Liu, W.; Wang, M. *Ceramics-Silikaty*.**2009**, *53*(2), 113-117.

54. Weitkamp, J.; Puppe, L. *Catalysis and Zeolites: Fundamentals and Applications*. Springer Verlag: Germany, **1999**.

55. West, A. R. *Solid State Chemistry and its Applications*. John Wiley and Sons: New York, **1996**, 4-115.

56. Byrappa, K.; Ohachi, T. *Cystal Growth Technology*. William Andrew Publishing: New York, **2003**.

57. Schubert, U.; Husing, N. *Synthesis of Inorganic Materials*. WILEY-VCH: Germany, **2005**.

58. Parr Instrument Company. *Operating Instructions; Parr Acid Digestion Bombs.* Illinois, USA, **1999**.

59. West, A. R. *Solid State Chemistry and its Applications*. John Wiley and Sons: New York, **1996**, 4-115.

60. Settle, F. A. *Handbook of Instrumental Techniques for Analytical Chemistry*. Prentice Hall PTR: New Jersey, **1997**.

61. Cullity, B. D. *Elements of X-ray Diffraction, 2nd ed.* Addison-Wesley: Menlo Park, **1978**.

62. David, W. I. F.; Shankland, K.; McCusker, L. B.; Baerlocher, Ch. *Structure Determination from Powder Diffraction Data*. Oxford University Press: USA, **2002**.

63. Smart, L.; Moore, E. *Solid State Chemistry: An Introduction*. Nelson Thornes Ltd: Cheltenham, **2001**.

64. http://serc.carleton.edu/research_education/geochemsheets/techniques/XRD.html

65. Pecharsky, V. K.; Zavalij, P. Y. *Fundamentals of Powder Diffraction and Structural Characterization of Materials*. Springer Science and Business Media, Inc: New York, **2005**.

66. http://serc.carleton.edu/research_education/geochemsheets/techniques/SXD.html

67. Campana, C. F. *Analytical Application Note: Single Crystal Diffraction*. Bruker AXS Inc: Madison, **2000**.

68. Bruker AXS. *M86-Exx078 APEX2 User Manual*. Bruker AXS Inc: Madison, **2006**.

69. http://serc.carleton.edu/research_education/geochemsheets/SREF.html

70. Otwinowski, Z.; Minor, W, *Methods in Enzymology*, in: Carter Jr, C. W.; Swet, R.M, (Eds.), *Macromolecular Crystallography part A, vol. 276*. Academic Press: USA, **1997**, 307-326.

71. Sheldrick, G. M. *Acta Cryst*. **2008**, *A64*, 112-122.

72. Hahn, Th. (Ed.). *International Tables for Crystallography, vol C*. Kluwer Academic Publishers: Holland.

73. Skoog, D. A.; Holler, F. J.; Crouch, S. R. *Principle of Instrumental Analysis*. 6th ed. Thomson Brooks/Cole: Belmont, **2007**.

74. Albani, J. R. *Principles and Applications of Fluorescence Spectroscopy*. Wiley-Blackwell: New York, **2007**.

75. Ross-Medgaarden. E. I.; Wachs. I. E. Phys. Chem. C. **2007**, *111*, 15089-15099.

76. Fergusson, J. E.; Harris, G. M. *J. Chem. Soc*. **1966**, *A*, 1293-1296.

77. Bao, D. M.; Gu, Y. P.; Zhou, X. S.; Xu, S. X.; You, W. S. *Liaoning Shifan Daxue Xuebao, Ziran Kexueban.* **2003**, *26*, 59.

78. Rocchiccioli-Deltcheff, C.; Fournier, M.; Franck, R.; Thouvenot, R. *Inorg. Chem*. **1983**, *32*, 207-216.

79. Mosa, J.; Larramona, G.; Aparicio, M. *J. Membr. Sci*. **2008**, *307*, 21.

80. Juris, A.; Balzani, V.; Barigelletti, F.; Campagna, S.; Belser, P.; Von Zelewsky, A. *Coord. Chem. ReV.***1988**, *84*, 85.

81. Che, M.; Fournier, M.; Launay, J. P. *J. Chem. Phys*. **1979**, *71*, 1954.

82. Allcock, H. R.; Bissell, E. C.; Shawl, E. T. *Inorg. Chem*. **1973**, *12*, 2963.

83. Hagrman, P. J.; Hagrman, D.; Zubieta, J. *Angew. Chem. Int. Ed*. **1999**, *38*, 2638-2684.

84. Otsuka, T.; Takahashi, N.; Fujigasaki, N.; Sekine, A.; Ohashi, Y.; Kaizu, Y. *Inorg. Chem*. **1999**, *38*, 1340-1347.

85. Molinari, A.; Amadelli, R.; Andreotti, L.; Maldotti, A. *J. Chem. Soc*. *Dalton*. **1990**, 1203-1204.

86. Wu, C. D.; Lu, C. Z.; Zhuang, H. H.; Huang, J. S. *Inorg. Chem*. **2002**, *41*, 5636-5637.